FAST FAULT LOCATION METHOD FOR A DISTRIBUTION SYSTEM WITH HIGH PENETRATION OF PV

A Dissertation
Presented to
The Academic Faculty

by

Miguel Jimenez Aparicio

In Partial Fulfillment
of the Requirements for the Degree
Master of Science in Electrical and Computer Engineering in the
School of Electrical and Computer Engineering

Georgia Institute of Technology
December 2020

FAST FAULT LOCATION METHOD FOR A DISTRIBUTION SYSTEM WITH HIGH PENETRATION OF PV

Approved by:

Dr. Santiago Grijalva, Advisor
School of Electrical and Computer Engineering
Georgia Institute of Technology

Dr. Sakis Meliopoulos
School of Electrical and Computer Engineering
Georgia Institute of Technology

Dr. Lukas Graber
School of Electrical and Computer Engineering
Georgia Institute of Technology

Date Approved: November 16, 2020

To my family and to all the persons that have accompanied me during this journey

ACKNOWLEDGEMENTS

I would like to thank all the people that have been with me during the writing of this thesis. This year, 2020, has been unique not only because of the usual academic challenges, but also due to external circumstances that have changed our way of life.

First, I would like to thank my advisor, Santiago, for believing in me while I was still a name in his inbox. His guidance and confidence have turned this work into what it is now. I am very fortunate in having had you as a professor and as an advisor, and I appreciate all the advice you have given to me regarding academic, and more importantly, non-academic topics. Also, I would like to acknowledge Matthew and the entire Sandia National Laboratories team. Their contribution was essential for the development of this thesis and I am thankful for the valuable feedback I received while writing my paper.

Secondly, I would like to express my most sincere appreciation to my parents, Ramon and Loli, and the rest of my family. Without them and their hard work during their whole lives, I wouldn't be here. I hope that someday I will be able to do the same for them.

Finally, I would like to express my gratitude to Jose Antonio, Alvaro, and especially to Carlos and Cristian, who have accompanied me during this journey at Georgia Tech. You have become my family-away-from-family. It wouldn’t have been the same without you.

Thanks,

TABLE OF CONTENTS

LIST OF TABLES

LIST OF FIGURES

LIST OF SYMBOLS AND ABBREVIATIONS

SLG	Single-Line-to-Ground
3P	Three-Phase
CWT	Continuous Wavelet Transform
CNN	Convolutional Neural Network
PV	Photovoltaic
MPPT	Maximum Power Point Tracking

SUMMARY

Distribution systems with high levels of solar PV may experience notable changes due to external conditions, such as temperature or solar irradiation. Fault detection methods must be developed in order to support these changes of conditions. This thesis develops a method for fast detection, location, and classification of faults in a system with a high level of solar PV. The method uses the Continuous Wavelet Transform (CWT) technique to detect the traveling waves produced by fault events. The CWT coefficients of the current waveform at the traveling wave arrival time provide a fingerprint that is characteristic of each fault type and location. Two Convolutional Neural Networks are trained to classify by node and type any new fault event in each measuring device. The method doesn't require communication between them. The results show that for multiple fault scenarios and solar PV conditions, high accuracy for both location and type classification can be obtained, even in scenarios where measuring noise is present.

CHAPTER 1. INTRODUCTION

This chapter presents the context in which this thesis is developed and the importance that is has in the future large-scale integration of Distributed Generation in current power distribution systems.

1.1 Context

The location of faults across a power system and the protection of electrical components have always been critical tasks in power engineering. In order to ensure the secure operation of the grid, many different monitoring and protection devices have been deployed across the system to detect and locate the presence of faults in the shortest time possible, and to take the necessary actions to guarantee the safety of the rest of the system. If those actions are delayed, a fault could irreversibly damage a power device, and compromise the stability of the system in the most extreme cases.

According to [1], 80% of the interruptions in a distribution system are due to faults. The most probable causes are the contact between conductors or with the ground due to the wind, animals, or the breakdown of an electricity pole. Most of the faults occur on overhead lines [1]. However, other equipment, such as transformers or relays, could be involved as well. Energy quality and safety issues arise when a fault happens, posing a risk to both the equipment and human beings. Inevitably, a fault will lead to loss of power for the customers and possibly to expensive repairs. Therein lies the importance of a fast and accurate fault location methods.

Over the last few years, there has been growing interest in distribution systems that include Distributed Generation (DGs), such as generators, energy storage, PV systems, and wind farms. The integration of these resources challenges the traditional techniques that

have been used for fault location. Some techniques, such as those that depend on the variation of impedance, are no longer applicable since power flows in the distribution grid are no longer unidirectional [2]. Sources close to or at the load site can result in negative net demand, modifying the direction of the power flows. While in transmission systems measuring devices can be located at each end of the line, in distribution systems the large number of feeders makes widespread sensing impractical. All these factors contribute to increased complexity of the already difficult task of fault location.

PV systems are being deployed in distribution systems at a rapid pace. Therefore, systems with a high penetration of solar PV are becoming more common and must be designed carefully. PV systems have different protection devices used to ensure the safety of the device against inner faults. However, external faults can still damage the system and therefore, any fault must be removed as fast as possible.

The contributions of this thesis are, first, a fault detection method that uses sudden magnitude differences in the coefficients of the Continuous Wavelet Transform (CWT) matrices of the current signals, with a Deep Learning algorithm based on Convolutional Neural Networks (CNNs), which is employed to classify both fault location and type. Both tools, CNN and CWT, have been employed either independently or jointly in the literature for fault detection and classifications purposes, though the combination of this detection method, the signal processing stage, and the obtained outcome of the classification algorithm makes this thesis a valuable research.

The second contribution of this thesis is to demonstrate that fault classification can be successfully accomplished on systems with high penetration of solar PV using the aforementioned method. For this purpose, fault signals under several PV conditions have been simulated. A case study on the IEEE 34 bus case has been prepared to draw conclusions.

1.2 Objectives

The objectives of this thesis can be listed as follows:

- Simulating faults in a power distribution system with high integration of solar PV.
- Developing a fast fault detection method that can perform a reliable detection in a period of time of a few milliseconds.
- Developing a reliable Machine Learning or Deep Learning algorithm to accurately classify locations and types of faults.

CHAPTER 2. LITERATURE REVIEW

Several approaches have been proposed for fault detection in distribution power systems, which can be classified in three main groups: analysis of voltage and current phasors and line impedance, methods based on detection of traveling wave or their properties, and techniques derived from Machine Learning and Artificial Intelligence algorithms.

The first group of techniques consists on monitoring several measurements, such as voltage, current or impedance, and use pre-fault and post-fault values to determine the location and the type of the fault. These methods have been widely used on transmission systems and are the working principle of distance relays that works with impedance. When a fault occurs, there is a change in the X/R impedance ratio that can be employed to determine the distance to the fault. The application of these methods on distribution systems may not be so accurate, but there have been attempts in this direction. The research in [1] employs the induced phase shift between the voltage and the current when the impedance ratio changes to determine which phases are involved in the fault and whether it is a grounded or ungrounded fault.

The second group of techniques relies on the identification and study of the properties of the traveling waves. When a fault occurs on a power line, a wave with a wide spectrum of frequencies and a velocity close to the speed of light propagates towards both ends of the line starting from the fault origin point. The range of frequencies can reach to several MHz. However, the characteristics of the line affects the propagation of the traveling wave: the wave experiments some attenuation, which reduces its frequency components and their velocities. In addition, different frequency components propagate at different velocities – larger frequencies imply larger velocities – which is the cause of the

dispersion of the wave. In literature, the wave is usually decomposed into three independent modes – a ground mode and two aerial modes - using the Karrenbauer transformation or Clarke transformation in order to decouple the electromagnetic coupling effects between lines [2]. The ground mode is more affected by attenuation and has a lower range of frequencies, which produces a more dispersed waveform that arrives later than the aerial modes and has a lower velocity. Some methods, as [3], take advantage of the time differences between modes and the velocity of the waves to calculate the distance to the fault. On the other hand, other methods use the time differences between consecutive reflections of the traveling wave with the fault point or with the end of the line [4]. The arrival time is generally obtained use the Continuous or the Discrete Wavelet Transformation (CWT/DWT), that relates the frequency and time domains. A sudden increase of the coefficients of the most sensitive scale (which is related with the highest frequencies of the wave) is characteristic of the arrival of a traveling wave.

Another approach using traveling waves is to use the characteristic frequencies of the wave. This research [5] shows that the parameters and length of each path will affect the frequency and velocity of the traveling wave in a distinctive way. Calculating the energy of the CWT at the arrival time, it is possible to infer the dominant frequency components of the traveling, that reveals the path followed by the wave. Once this path is found, the location of the fault is determined by a calculation that involves time differences between consecutive traveling waves arrivals (due to reflections) and the length of the path. In order to reveal all the characteristic frequencies of the traveling wave, it is better to use a mother wavelet that it is inferred from the actual wave [6].

The third group of techniques is composed by all those Machine Learning or Artificial Intelligence techniques that can be applied to detect and locate faults in power systems. A constant in the literature is separation between algorithm that classify the faults

(i.e., type, section, resistance) and the algorithms that locate the exact location of the fault across the line or node.

Regarding the classifier algorithms, there have been attempts to apply Fuzzy Inference Systems (FIS) to determine the fault scenario. For example, in [7] the calculated energy for the CWT coefficients in a per-phase approach for current and voltage after a fault is used to establish which phases have been involved in the fault. In [8], the fault resistance is inferred supposing that the fault type is known and that the estimated distance to the fault is given by two distance relays, each one located at each side of the line. Other projects use Support Vector Machine (SVM) to determine the fault features. In [9], the energy of the DWT coefficients of the 3-phase voltages is used to determine if each phase is involved in the fault and if the line is faulty or not. The limit of SVM classifiers in more complex systems is the fact that the output is binary, so each classifier is trained to give a yes/no answer to the input. On the other hand, [10] uses an Artificial Neural Network (ANN) to determine the faulty section in a small distribution system. The output of the network gives a binary code that refers to each of the sections of the grid. The research in [11] uses a Multi-Layer Perceptron (MLP) Neural Network, a special type of ANN, to infer the fault resistance in a transmission line. It employs the ratios of fault voltage and current in per unit referred to pre-fault values.

However, more advanced classifiers use Convolutional Neural Networks (CNNs), which are a powerful technique used for example, in image recognition because of its great capability of extracting features. Given an image, a CNN can divide it into small segments and detect the most important features. In addition, the CNN does not need to perform complex operations, such as CWT or DWT, to extract those features. In the case of [12], the CWT coefficients of the transient zero-sequence current at each bus are used as an image, and the output is the faulty feeder. According to their research, results are better with CWT than with DWT. It is also stated that the proposed method is more accurate than

using a SVM or an Adaboost classifier. This research shows that this method is resilient to noise interference, network changes and several inception angles and resistance values.

CNNs has also been used for one-dimensional arrays with excellent results. In [13], this type of network has been used to detect the faulty section of an HVDC line. The input is the high frequency components of the fault signal at the inverter and the rectifier sides, which has been extracted using the Empirical Mode Decomposition (EMD). This research remarks the importance of parameter optimization for achieving an accurate performance of the CNN, but it also remarks its superiority in comparison with other classification techniques, such as SVM. Another approach [14] uses Adaptative Convolutional Neural Networks (ACNNs) to process the 3-phase current measurements two cycles before and after the fault in order to get the fault type and if the fault is internal or external to the line. This method assumes that measurements from two Phasor Measurement Units (PMUs), each one at each side of the line, are available. The most important conclusion that can be drawn from this study is that ACNNs are trained faster that CNNs, have a slightly better accuracy while maintaining the excellent performance of CNNs regarding changes in the grid, in the fault resistance, inception angle, etc.

In relation to the algorithms that are able to find the exact location of the fault, the algorithm introduced in [3] applies fuzzy logic to the distance to the fault that has been estimated by four different measurement devices. In addition to the four estimations, the faulty section is also an input. The method claims to be accurate for a distribution system even in a scenario with Distributed Generation (DG). In [15], a Recurrent Neural Network (RNN) is used to infer the location of the fault using the difference between the traveling wave arrival times to three different devices, each one located at each one of the buses that compose the system. The RNN is trained to find the location of the fault based on the combination of arrival times. In [9], the procedure is similar, but they use the differences in arrival times of the 3 first traveling waves and its polarity. In [16], the method considers

a MLP neural network. The input is the variation of the first scale coefficients of the DWT along time and it is proven to work for a transmission line. One approach that it is important to mention is the one developed for a transmission line in [17], which employs a special type of ANN called Extreme Learning Machine (ELM). This algorithm performs fault classification and location at the same time, but it requires a fault detection algorithm first. The input of this neural network is just a single cycle of current waveform, with any other pre-processing apart from normalization. In this research, the algorithm is expanded and integrates wavelet and gaussian activation functions to extract features in each neuron. This method is really called "summation-Gaussian ELM." To perform the fault location, the SG-ELM has to perform a regression task. The output of the algorithm has an integer part that indicates the type of fault, and a decimal part that determines the actual location of the fault as a percentage of the line length.

CHAPTER 3. PROPOSED METHOD

The goal of this chapter is to develop a method capable of detecting a fault, either if it has been produced on a node with solar PV or not, and infer the fault scenario (i.e., the fault type and location). Measuring devices located across the system will be trained to perform this classification. In practice, each device will be able to independently protect their area of influence. Techniques such as Continuous Wavelet Transform (CWT) are used to analyze the fault signal, and Convolutional Neural Networks are trained to perform the classification of the faulty node and type.

In the first place, faults are simulated in PSCAD, which is a time domain simulation software whose capabilities include electromagnetic transient simulations. This software allows to simulate the fault transients, which is the data that will be used for classification. A custom distribution power system based on the IEEE 34 bus case, with three solar PV farms, is modeled. It is the standard benchmark that is used throughout the project.

As a brief introduction to the algorithm, after the faults have been simulated, there are two main stages: the data processing and feature extraction stage, and the actual CNN model training stage. The first stage goal is to provide a standard quantitative fault representation that can be used later to compose a training set of different faults in equal circumstances. In the first place, the designed algorithm identifies whether if a fault has occurred or not in the recorded current measurements. For this purpose, an analysis based on the Continuous Wavelet Transform, that represents signal frequency over time, is used to determine in which point of time the signal carries a larger amount of high frequencies (which is a clear indicative of the existence of a fault). It is important to note that for this stage, the 3-phase current measurements are decomposed into 3 independent modes using the Karrenbauer transformation and the ground mode is used.

Faults are simulated at some of the nodes of the designated test system and the measurements taken by some devices located across the system are analyzed to check the existence of a fault. One of the desirable features of fault detection is speed. Thus, a measurement sampling frequency of 10 MHz is used, and the data is processed every 0.1 millisecond (every 1000 samples). Such a small period of time implies that the decision of whether a fault has occurred or not will not be based on the whole fault transient, but rather it will be based only on the first part of the fault dynamics: the traveling waves.

Once the exact traveling wave arrival time is determined, the signal is cropped 0.5 milliseconds (ms) before and after this time. The 1 ms time window provides a long-enough benchmark that includes sufficient information about the fault dynamics and will allow a reliable fault classification. The training set is not composed by this raw 1 ms signal, but it is composed by the CWT matrices associated to it. These matrices provide an extremely valuable feature to work with, as they are not focused on the plain values of the fault current, but it contains all the information regarding the inherent frequencies of the waves.

Afterwards, the Machine Learning models employs convolutional neural networks, largely used in image classification, to unveil and learn features that are present on the CWT matrices. The suitability of this approach is clear: on the one hand, CWT is an extremely powerful signal processing tool that allows to the exact arrival point of the high frequencies. In the context of fault detection, this approach outperforms other Fourier-based tools that would only give information about the existing frequencies in a certain period of time. On the other hand, it is consistent with the theory of propagation of the traveling waves, that states that the frequency components of a traveling wave are attenuated during the wave propagation across the line. This attenuation depends on the line impedance and increases with the distance (specially for the ground mode), which suggests that theoretically different propagation paths and fault locations would lead to different measured frequency components. This is the base upon the classification is made.

For this reason, the CWT matrices, which contains all the information regarding frequency components over time, are used to train the Machine Learning models. These matrices are quite large and can be treated as images (indeed they are usually represented as images). This makes CNN a perfect tool to analyze them and identify any underlying pattern on the frequency components.

CHAPTER 4. TEST SYSTEM AND FAULT SIMULATION

This chapter aims to define the test system and provide information regarding the fault locations and other simulation parameters.

4.1 The test system

The system selected to perform the fault simulations is the IEEE 34 node case, which is available in PSCAD format [18]. The simulations were performed with this software tool using the Automation Library for Python. The system is illustrated in Figure 1, which presents the circuit topology, and main devices, as well as location of PV system and faults (whose location is to be detected).

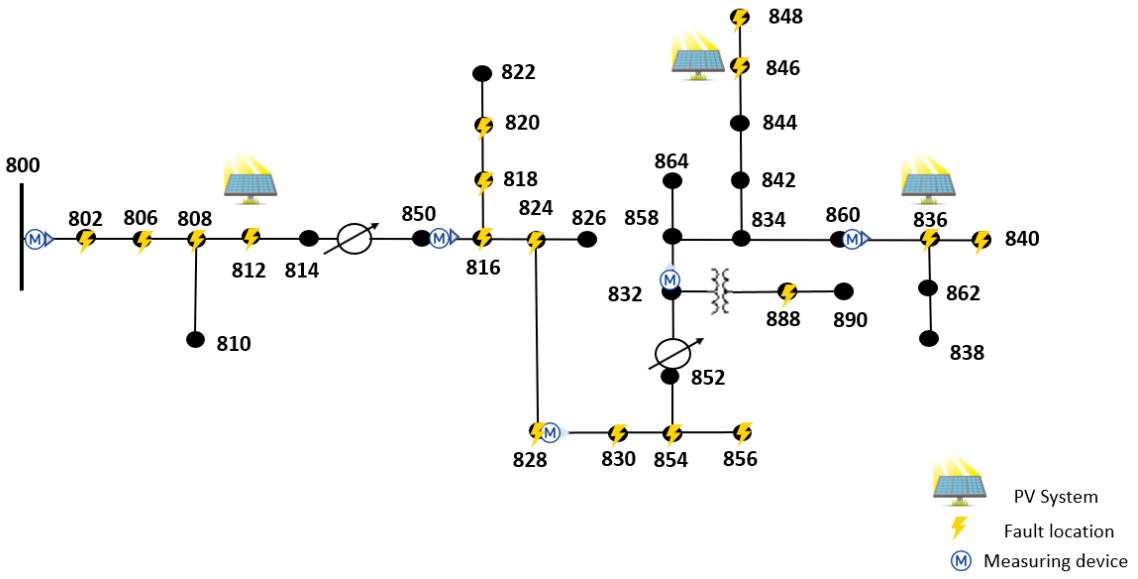

Figure 1. Test systems including locations of PV systems, faults and measuring devices

4.1.1 System features

The system has the following features:

- 34 nodes (node 800 corresponds to the substation).
- 16 fault locations, which are located in nodes: 802, 806, 808, 812, 816, 818, 820, 824, 828, 830, 854, 856, 840, 848, 846 and 836.
- 3 PV systems on nodes: 812, 836 and 846.
- 5 measuring devices that record 3-phase current at a sampling frequency of 10 MHz. These devices are located in nodes: 800, 850, 828, 832 and 860.

The distribution lines of the circuit have been modeled in a way that the frequency-dependent (phase) model available on PSCAD can be used for performing the simulations. The usage of this model is of special importance in order to obtain an accurate representation of the traveling waves, as the propagation of each of its frequency components depends on the line characteristics. In order to model the lines, the information available in [19] and [20] was employed to define the line spacing, the line length and the line impedance in PSCAD.

4.1.2 Solar PV System

The solar farm model was obtained from PSCAD [21] and it is used to represent the PV systems. This model is composed by the PV array, the boost converter, the inverter and an LCL filter to remove the harmonics. A more detailed overview of the model can be seen in Appendix A. There is an output active power control which is based on the Maximum Peak Power Tracking (MPPT) controller.

The inputs to this model are:

- Irradiation. Two values: 600 and 1000 W/m^2 are employed for the simulations.
- Temperature. Two values: 28 and 50°C are employed for the simulations.
- Output power reference, which is set to 200 kW (2 units of 100 kW each).
- Output voltage reference, which is set to 24.9 kV (1 p.u. in terms of the voltage base).

Irradiation and temperature have a great influence in the output power [22]. Higher irradiation allows to obtain larger output current (which translates into higher output power). On the contrary, higher temperature implies lower voltage in the PV array, which reduce the maximum output power that can be achieved. The output power is optimized by the MPPT controller, which adjust the boost converter parameters to provide the specified output power. Note that for certain conditions of irradiation and temperature it may not be possible to reach the reference of 200 kW. The values of irradiation and temperature fluctuate along the day (specially irradiation, which can be affected by clouds or dust). However, in this study, just a fix value for both parameters is taken in account for simulations as it is considered that a significant change cannot occur in the time interval of 2 milliseconds, which is the simulation time.

4.2 Fault Simulation

4.2.1 Fault parameters

As shown in Figure 2, two types of faults are taken into consideration in this project: Single-Line-to-Ground (SLG) faults, which are the most common type of faults according to [1], and Three-Phase (3P) faults, which are the most severe types of faults.

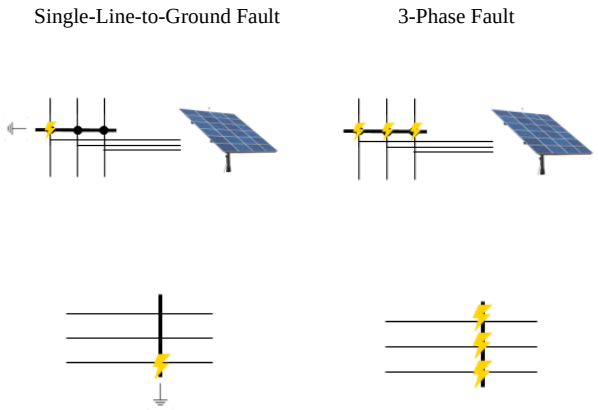

Figure 2. Simulated faults for nodes with and without PV systems

In addition, each fault is simulated using 4 different resistant values: 0.01, 0.1, 1 and 10 Ω. Taking in account the different fault types (SLG and 3P), resistances (4 values) and locations (16 nodes) and the four different PV scenarios that are draw from the two values of irradiation and temperature (600 W/m^2 and 28°C, 600 W/m^2 and 50°C, 1000 W/m^2 and 28°C and 1000 W/m^2 and 50°C), the total number of fault simulations is 464.

4.2.2 Simulating faults in PSCAD

The process of simulating the faults in PSCAD involves two stages, which can be appreciated on Figure 3.

- Transient to steady state: The system without any fault is simulated for 2 seconds, which is enough for ensuring that it arrives to the steady state. The time step is 0.1 μs, which is consistent with the desired sampling frequency of 10 MHz. After 2 seconds, a snapshot is made saving the state of the system in that specific moment.
- Fault transient: Taking a snapshot as the starting point, 2 milliseconds are simulated. The fault occurs at 1 ms. Therefore, approximately the first half of the measurements records the system during normal operation, while the second half shows the incipient fault current transient.

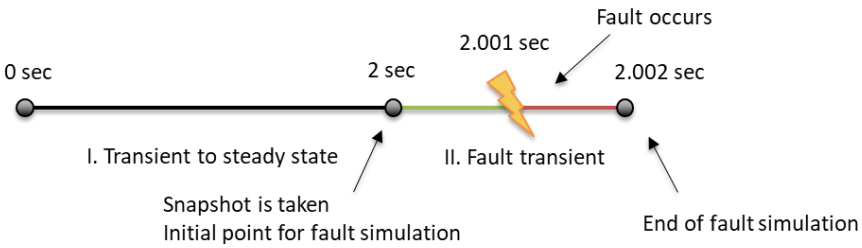

Figure 3. Stages and chronogram for fault simulation in PSCAD

The output of each simulation is a group of signal measurements, from which the 3-phase current recordings of each of the 5 multimeters located across the system are used. For a total simulation time of 2 ms and a sampling frequency of 10 MHz, 20000 data points are recorded for each current.

CHAPTER 5. DATA PREPARATION

The first stage of the data preparation and feature creation stage involves the detection of a sudden transient in the 3-phase current that would indicate the existence of a fault somewhere in the circuit. This initial stage requires the decomposition of the 3-phase current into three different independent modes (the ground mode and two aerial modes) using the Karrenbauer transformation [23]. The transformation can be appreciated in Equation 1.

$$\begin{bmatrix} I_0 \\ I_\alpha \\ I_\beta \end{bmatrix} = \frac{1}{3} \begin{bmatrix} 1 & 1 & 1 \\ -1 & 0 & 1 \\ 0 & -1 & 1 \end{bmatrix} \begin{bmatrix} I_A \\ I_B \\ I_C \end{bmatrix} \quad \text{Eq. 1}$$

The ground mode I_0 allows to easily observe any disturbance that may have been caused by a fault. During normal operation, it should be around 0 Amperes as the current phasors cancel among themselves (supposing an almost balanced system). However, any fault will cause a perturbation that will put the ground mode current away from this 0 Amperes level. Therefore, even when the phase current amplitudes are large, the ground mode current will reveal a fault transient from the very beginning. Also, the ground displays some important properties regarding fault waveform propagation across the circuit. Ground mode is much more affected by attenuation, so it is very sensitive to distance. The inherent information that it contains (in special regarding the frequency components) will be a great aid for distinguishing between faults in different locations.

The fault detection and the later fault classification method have been both tested for cases with and without noise. For simulating a measuring noise, a gaussian noise with variance proportional to the steady state current amplitude is added to the 2 ms measured

signal. The approximate steady state current amplitude in each of the nodes where the measuring devices are located is included in Table I.

Table I. Approximate Steady State Current Amplitude

MULTIMETER	CURRENT AMPLITUDE (AMPS)
Substation	60
1	60
2	50
3	30
4	10

In Figure 4, two recorded signals, one with noise and one without noise, are shown. Faults signals correspond to a 3P fault in the node 806 and have been measured by multimeter 1 (in node 850). The fault scenario involves a fault resistance of 0.1 ohm, and the solar conditions are an irradiation of 600 W/m^2 and a temperature of 28°C.

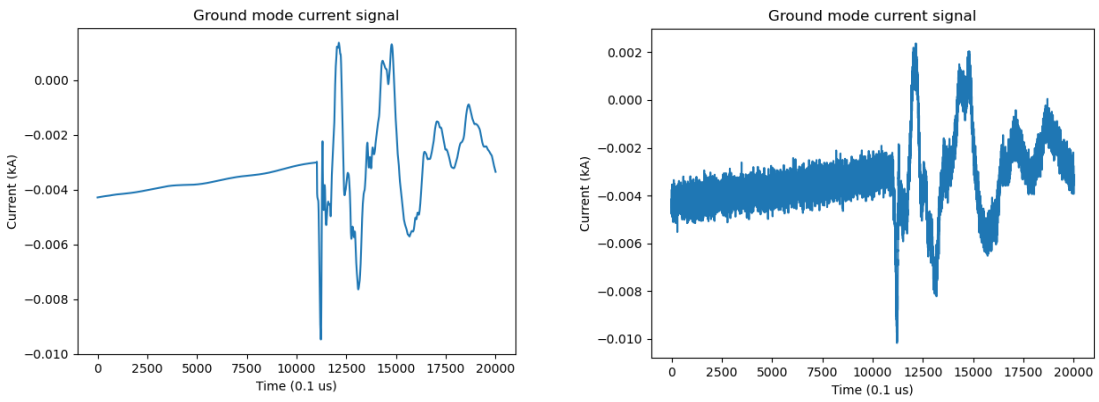

Figure 4. Current signals and Travelling Waves without and with measuring noise (left/ right)

The signal is later divided on non-overlapping slices of 0.1 ms. This resembles the operation of an actual protection device that is continuously measuring and analyzing the data. Using windows of 0.1 ms allow a fast fault detection as less data need to be gathered before it is analyzed. The workflow of this part of the algorithm is shown on Figure 5.

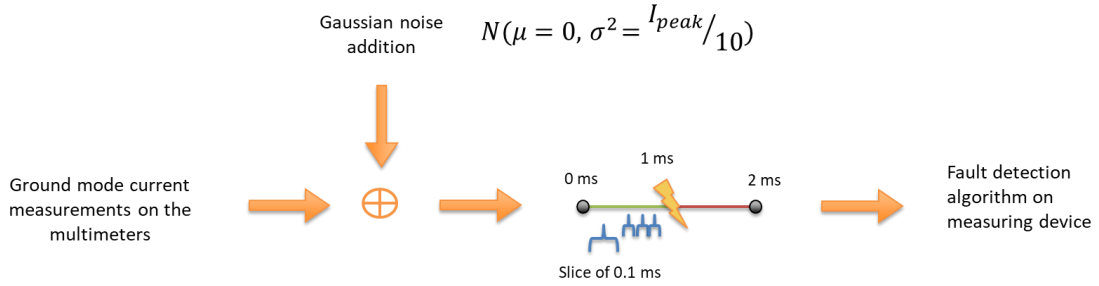

Figure 5. Detail of the pre-processing stage that illustrates the noise addition and the signal slicing

Such a small period of time implies that the decision of whether a fault has occurred or not will not be based on the whole fault transient, but rather it will be based only on the first part of the fault dynamics: the traveling waves.

5.1 Fault detection

The input of the fault detection stage is the previously obtained 0.1 ms slices. For the cases with noise, a smoothing filter that uses a Hanning window is employed to filter out the high-frequency components related to the noise. The length of the signal is 1000 data points and the smoothing window length is chosen to be 500 samples.

The working principle of the fault detection algorithm is the Continuous Wavelet Transform (CWT) and the relative changes in the coefficients' magnitude, which could indicate the presence of a fault.

5.1.1 The Continuous Wavelet Transform

The Continuous Wavelet Transform (CWT) is a powerful signal processing tool that is used to analyze the frequency components of a signal along a period of time. In this transform, the signal is split into frequency components, which are evaluated for different scales. This method can provide high-frequency resolution for low scales, which is needed to determine the arrival time of the traveling wave.

The mother wavelet ψ(t), which in this case is the Morlet wavelet, is scaled by the scale coefficient *a* and translated by the translation coefficient *b*. The CWT of the signal x(t) is then defined by [12], and it is shown in Equation 2.

$$CWT_x(a,b) = \frac{1}{\sqrt{a}} \int_{-\infty}^{\infty} x(t)\, \psi\left(\frac{t-b}{a}\right) dt \qquad \text{Eq. 2}$$

The CWT of a signal returns a matrix whose rows (also referred as scales) are frequency components. The first scale is related to the highest frequency component that is actually measured and, from there, a larger scale implies a lower frequency. Columns of the CWT matrix are the time data points. Therefore, this matrix is a representation of frequency against time. Larger coefficient magnitudes are an indicative of a higher importance of that specific frequency component.

For the fault detection algorithm, the first scale is used. The disturbance caused by a fault event will produce a sudden change in the ground mode current, which will be translated into a magnitude increase of the higher frequency components of the signal.

5.1.2 The detection algorithm

Therefore, monitoring the coefficients of the first CWT scale, it is possible to evaluate the existence of a fault. As it can be appreciated on Figure 6, a constant padding is applied to the signal before performing the transformation. This avoid having edge-effects that could mislead the next stage of the algorithm.

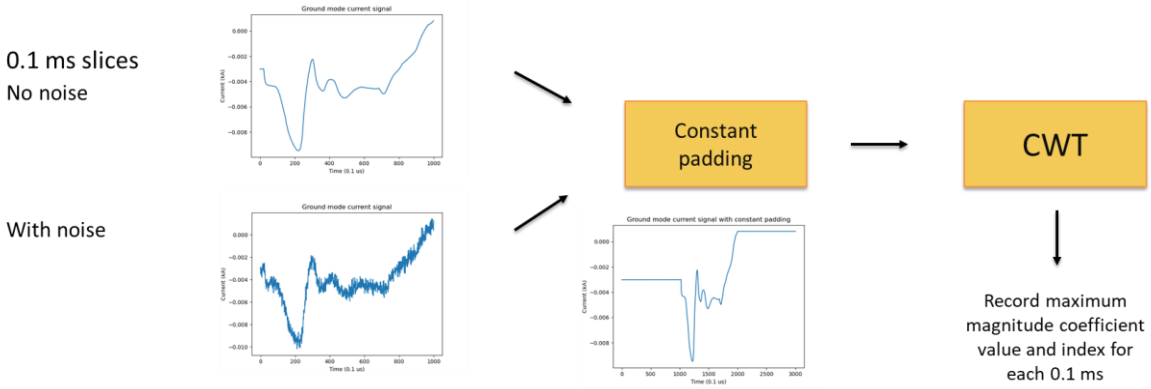

Figure 6. Application of constant padding before the CWT

Once the transformation is performed, the maximum magnitude coefficient value and index is recorded for each 0.1 ms slice. A statistical analysis similar to the Z-score test is employed to determine if a fault has been detected (this conclusion is reached when a new data point is too far from the given distribution of points). Regarding this test, when a point is more than 4 standard deviations away from the average, it is considered as an outlier. Therefore, for each new maximum magnitude coefficient value, it is calculated whether if it is an outlier or not. If the answer is positive, a fault has been detected and the index is considered as the ground mode traveling wave arrival time. If not, the average and the standard deviation are recalculated using this new data.

In Figure 7, the maximum magnitude coefficient values and indexes for a few consecutive 0.1 ms slices are shown. After approximately 1 ms, a huge jump in magnitude

has been observed. This indicates that a fault must have occurred. The index of the last point is considered as the ground mode TW arrival time.

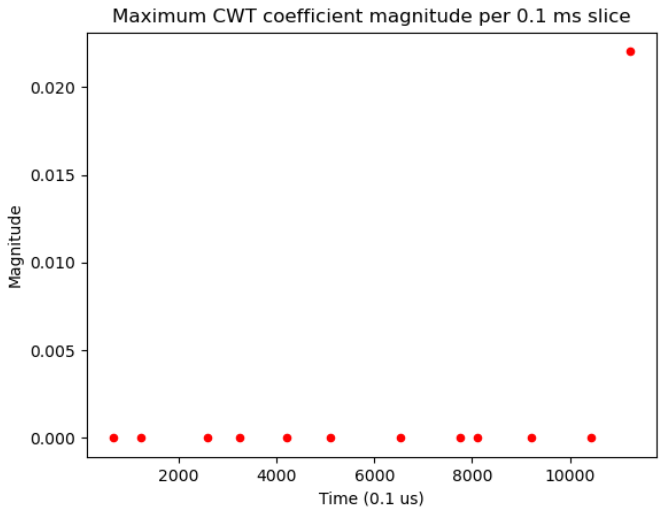

Figure 7. Maximum magnitude of a first scale CWT coefficient along consecutive 0.1 ms periods

In order to have a common benchmark for the training process, the ground mode current waveform is cropped 0.5 ms before and after the ground mode arrival time, and the CWT of that 1 ms signal is saved for the training of the CNNs. It is important to notice that even though the signals are analyzed every 0.1 ms, a little bit more of data is gathered before performing the final CWT. This allows getting a more complete representation of the traveling wave, which helps in the classification task. In Figure 8, two examples of the final 1 ms signals and their respective CWT can be observed.

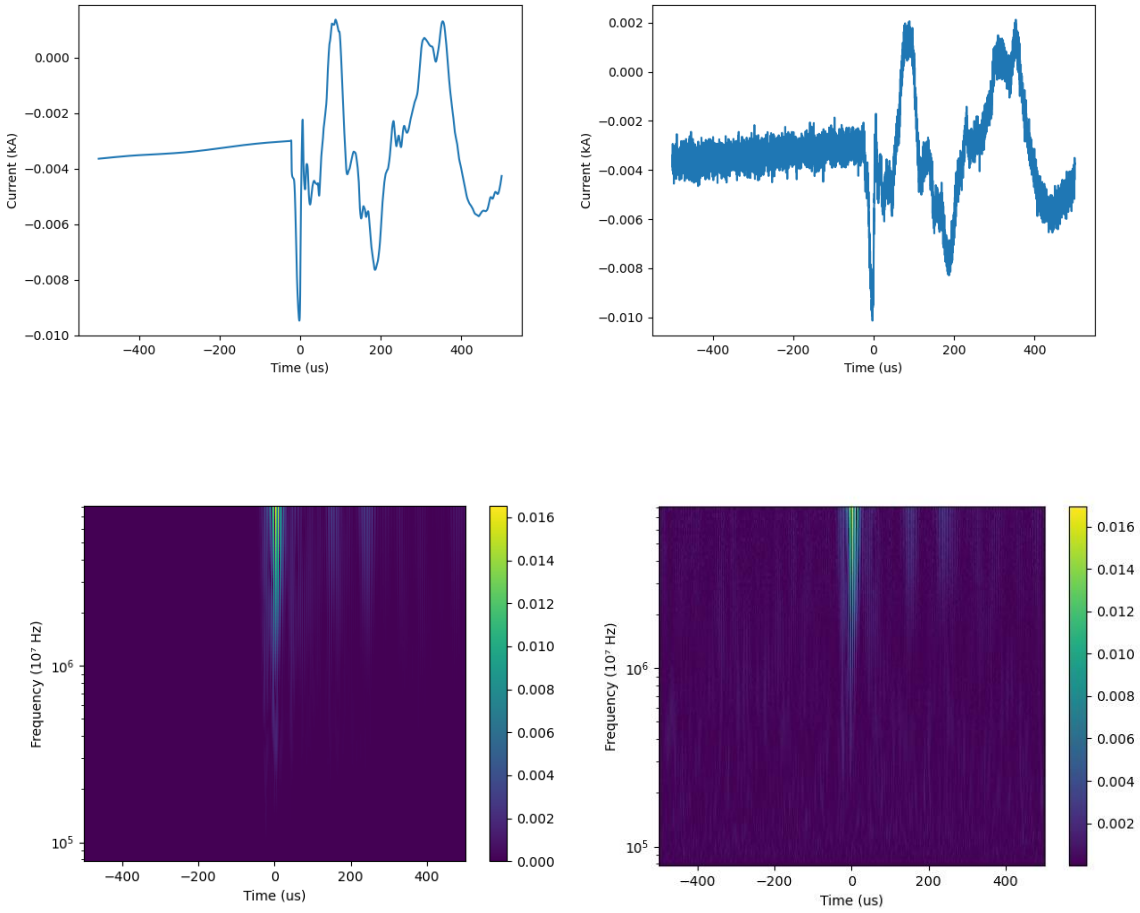

a) Without gaussian noise *b) With gaussian noise*

Figure 8. CWT coefficient matrices of a signal without/with added noise

Around 0 us, which is the TW ground mode arrival time, it is possible to see a huge increase on the coefficient magnitudes. This is especially noticeable on the highest frequencies (lower scales). Also, for the case with noise, some background white noise can be appreciated across all the frequencies in the matrix.

CHAPTER 6. MODEL TRAINING

Given that simulated faults are labelled, a supervised algorithm is going to be used for the training process. Otherwise, it could be difficult to address which patterns in the data actually refer to changes in location or type and which patterns are due to other conditions, such as resistance, irradiance, etc. For this project, a Convolutional Neural Network is the chosen algorithm for its suitability and superior performance in image classification. In practice, the CWT matrices can be treated as images. One CNN is trained for node classification, and another one for type classification.

6.1 Convolutional Neural Networks

Convolutional Neural Networks are composed by a structure of successive layers: convolutional layers, maximum pooling, average pooling, dense, etc. The first type, the convolutional layers, are called in that way because the main operation that takes place is the convolution.

This operation is used to extract information from the image while maintaining the spatial relationship of pixels. The convolution is done between the original image and a defined kernel or filter. This operation consists of the consecutive dot products between the kernel and a portion of the image. The result is saved into a matrix. The matrix is filled up with successive iterations of this operation across the whole input image. The resulting matrix is called a "feature map." Depending on the filter, the feature map will be different. The value of these filters is what it is learned during the training process.

The size of the feature map will depend on the size of the original image and on the size of the filter. Also, it depends on how the kernel is moved across the matrix. For this application, the kernels are much smaller than the original images, so the feature maps will

almost have the same size. It is preferable to use small kernels as they are more sensitive to image details.

Another important parameter to take in account is the activation function. For the convolutional layers, the ReLU function is employed, which is basically to change any negative number in the feature map by zero. In this way, non-linearity is introduced as reality is non-linear.

Both average and maximum pooling layers are really a downsampling of the input map. They are aimed to gather the most relevant information. Pooling layers require to specify a matrix size and the feature map in divided in regions of that size. Then, for a maximum pooling layer, only the maximum value of each region is saved. Instead, for an average pooling layer, the average of the region values is saved. Following the same reason as before, the regions have a small size to maintain the details of the input feature map.

Convolutional and pooling layers are carefully assembled to extract the most important data from the image and to reduce feature dimension. In Keras, which is the selected deep learning library for this project, “dropout” layers are also included in between to avoid overfitting. Basically, this type of layer drops to 0 the output of the specified percentage of neurons.

The last step is a dense layer (also called fully connected layer) where the neurons in the layer are connected to all the neurons in the previous layer. The number of neurons in the dense layer is the same as the number of possible outcomes. For example, for node classification, there will be as many neurons as possible locations. For type classification, there will be as many neurons as possible types. As the CNNs are dealing with matrices

and a dense layer is a 1D array, a flatten layer is included before to convert the input maps into a one-dimensional array. The employed CNN structure for both node and type classification can be appreciated in Figure 9.

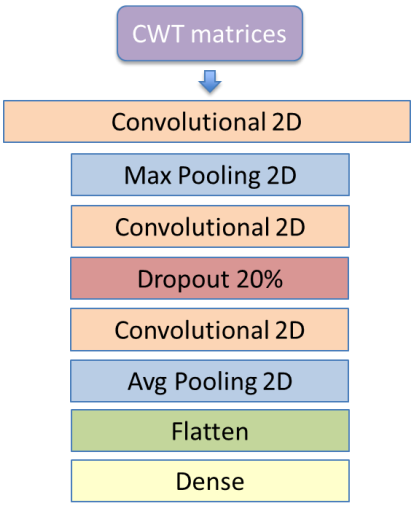

Figure 9. Layer structure of the Convolutional Neural Networks

6.2 Training Process

Out of the 464 faults (which produce the same number of matrices of coefficients), 348 of those matrices of coefficients actually compose the training set. The remaining 116 matrices are used for the test set. The size of each matrix is 104-by-10000, where 104 is the number of scales and 10000 the number of samples that is obtained in 1 ms at 10 MHz. However, in order to reduce the required computation effort and the resources needed to train both CNNs, a down-sampling with a factor of 100 was used in order to reduce the size of the obtained CWT coefficient matrices. Therefore, the training set is composed by matrices of size 104-by-100. It is important to notice that each fault is measured by 5 different multimeters, and each multimeter will be trained using their own measurements.

For the node classification, the labels that are used for training are just the node labels (Ex: ‘802’, ’836’...) and there are 16 different labels. For type classification, the labels are just the fault types (either ‘SLG’ or ’3P’).

As mentioned before, the layer structure of both the type and node CNN is identical. The number of neurons in each layer is the same for both neural networks, except for the last layer, which for node classification has 16 neurons and indicates the most probable location, and for type classification has 2 neurons and indicates the most probable type. A detailed description of the CNN layer structure can be found in table II.

Table II. Configuration of each CNN layer for node (type) classification

LAYER TYPE	KERNEL SIZE	OUTPUT SIZE	ACTIVATION FUNCTION
CONVOLUTIONAL	5 x 5	100x96x104	ReLU
MAX POOLING	-	50x48x104	-
CONVOLUTIONAL	3 x 3	48x46x52	ReLU
DROPOUT 20%	-	48x46x52	-
CONVOLUTIONAL	2 x 2	47x45x26	ReLU
AVERAGE POOLING	-	23x22x26	-
FLATTEN	-	13156	-
DENSE	-	9 (2)	Sigmoid

For each of the 5 multimeters, a CNN for node and type classification are trained. Therefore, 5 node CNNs and 5 type CNNs are trained in total. The employed optimizer is Adam and the optimum learning rate and two beta parameters that define the momentum are determined by a grid search for each of them. The selected values for the grid search include the default value of the parameters and a couple of values close to it. In total, 25

combinations of learning parameters are tried, from which the one with maximum accuracy is chosen. Each CNN for each multimeter and for each classification target, either type or node, has it own optimum model that maximizes classification performance.

CHAPTER 7. MODEL EVALUATION

This chapter provides the numerical results for node and type classification in scenarios with and without noise. First, node classification is going to be presented for both scenarios, followed by some comments about the observed results. Secondly, type classification will be analyzed in the same way.

The accuracy metric that is used is just the number of correct predictions divided by the total number of test set cases (which is composed by 116 faults). Each multimeter is assessed independently.

7.1 Node classification

7.1.1 Without noise

The following figure shows a multilabel confusion matrix for each multimeter in which the predicted nodes are plotted against the true nodes. Therefore, the expected result is that the prediction equals the node where the fault occurs, so that particular case falls on the diagonal of the matrix. For each fault location, the test set is composed by several faults' conditions (fault resistance values and irradiation and temperature conditions) that have not been shown previously during the training stage.

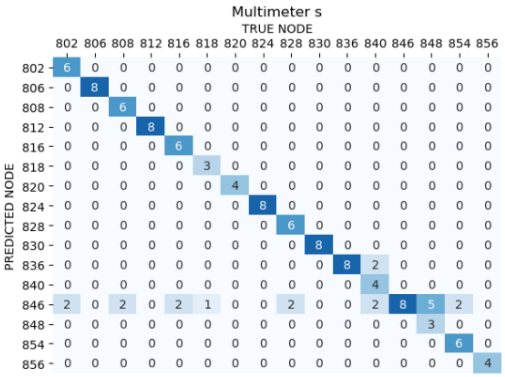

Accuracy: 82.75%

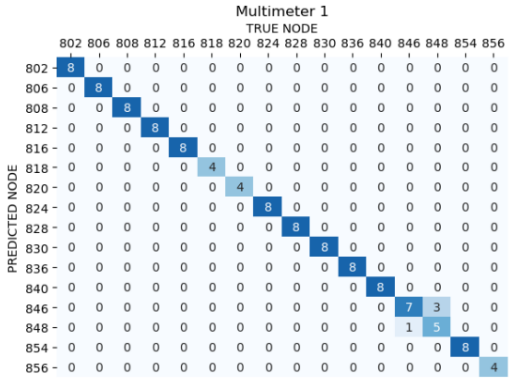

Accuracy: 96.55%

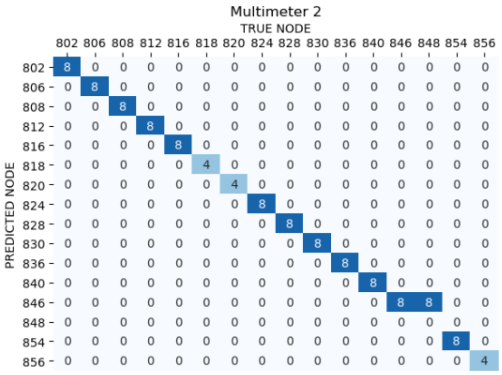

Accuracy: 93.10%

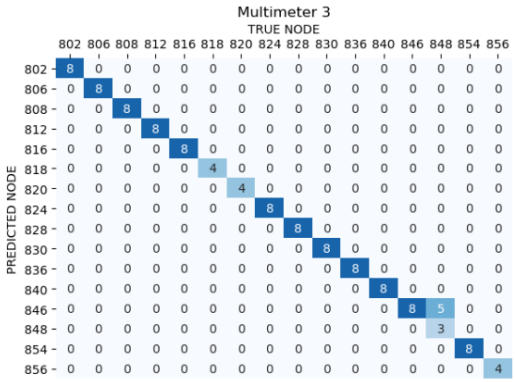

Accuracy: 95.68%

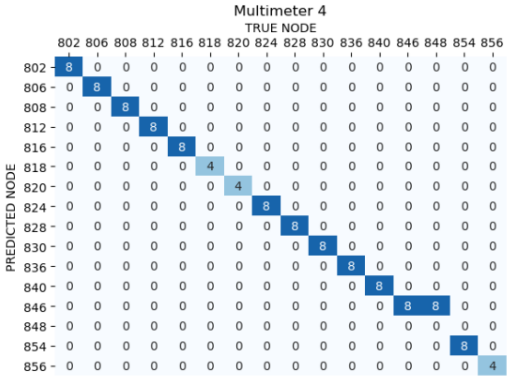

Accuracy: 93.10%

Figure 10. Node classification results for cases without noise

As it can be observed, accuracy is greater than 90% for the multimeters located across the distribution system and faults all over the system are consistently correctly classified. This shows the capabilities of the method. The accuracy for the multimeter located in the substation is a little bit lower, but it is still over 80%. This lower performance is directly related with the large distance to some faults situated in the other side of the system. Propagation and attenuation of the traveling waves may cause the frequency components to look similar among different faults. Therefore, classification of those faults becomes a harder task.

Another remarkable issue is that for all the multimeters, misclassification usually occurs for nodes 846 and 848. Those nodes are situated behind a capacitor bank located on node 844 (just before those nodes). One visible effect is that the measured traveling waves looks smoother than in other fault locations and the overall appearance is similar. Undoubtedly, this is going to make that the frequency components will look the same, and because of that the algorithm will find very difficult to classify faults in those two nodes.

7.1.2 With noise

As in the previous section, in Figure 11, five multi label confusion labels are presented. This time, for scenarios with noise, as explained on Chapter 5.

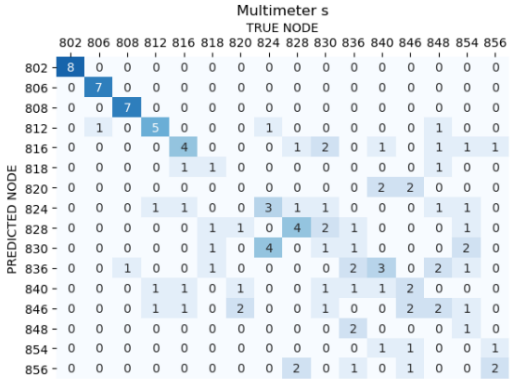

Accuracy: 40.51%

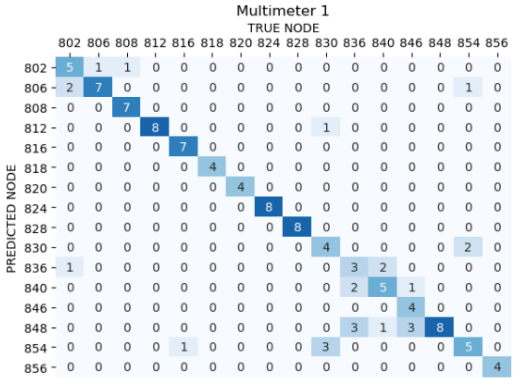

Accuracy: 78.44%

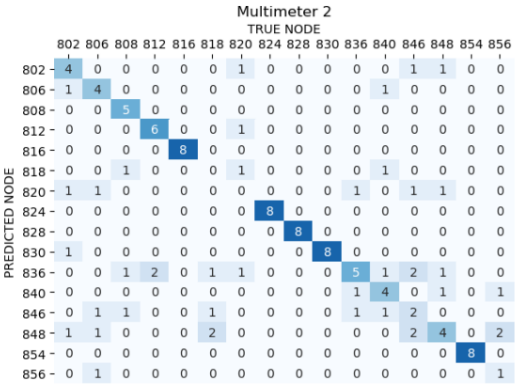

Accuracy: 64.65%

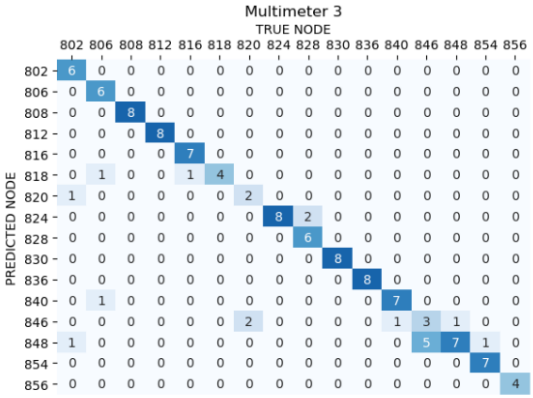

Accuracy: 85.34%

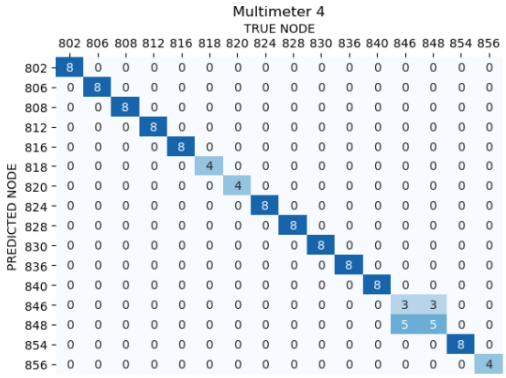

Accuracy: 93.10%

Figure 11. Node classification results for cases with noise

For cases with noise, it is possible to notice that the accuracy for the multimeter on the substation is significantly lower. The measuring noise, added to the attenuation of the signals, makes it really difficult to classify fault that don't occur on nearby nodes. For multimeters 1 and 2, which are located on nodes 850 and 828 respectively, accuracies are lower as well when comparing to the cases without noise. Faults that occur on far nodes located downstream in the system (for example, nodes 836, 846 or 848) seems difficult to classify and accuracies are significantly lower. This can be noticed on their respective confusion matrices, which show a remarkable dispersion on those nodes. However, for nearby nodes the accuracy is still high. In consonance, multimeter 2 shows a lower performance on nodes closer to the substation, while multimeter 1 does a great job there as it is remarkably closer.

For multimeters 3 and 4, performance don't seem to be extremely affected by noise, which is quite impressive. Accuracy for multimeter 3 is over 85%, just ten percent less than for scenarios without noise. This multimeter suffers more when classifying the farthest nodes, which are 802 and 806 (close to the substation) and 816, 818 and 820 (which are part of a distant branch). For multimeter 4, accuracy is the same as in the previous section.

7.1.3 Concept of protection zones

Results drawn from the analysis of scenarios with and without noise suggest that a real application would require an optimization of the multimeters positioning, as accuracy depends on location. As it was shown in the previous section, multimeters do a great classification task at least for the nodes that are close to them. This leads to the concept of "protection zones". This means that each multimeter could be effectively in charge of a few nearby nodes. In the current system, with the current multimeters location and the available fault information, the different protection zones are described on Table III.

Table III. Protection zones for each multimeter

Multimeter	Protected nodes based on accuracy	Overview of protection zone
s	Nodes 802, 806, 808, 812 and 816.	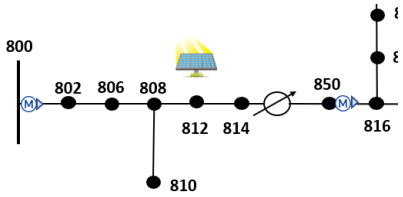
1	Nodes 806, 808, 812, 816, 818, 820, 824, 828, 840, 848 and 856.	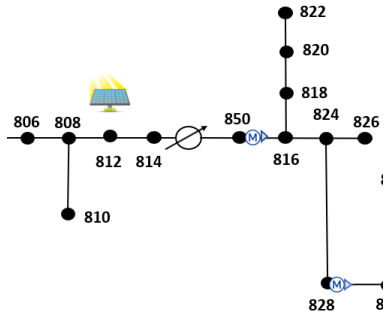
2	Nodes 812, 816, 824, 828, 830, and 854.	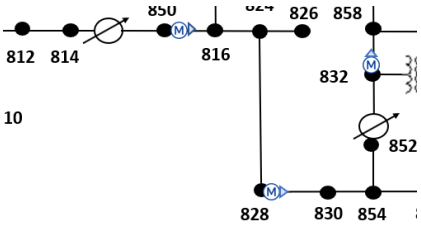
3	All nodes.	The whole system
4	All nodes.	The whole system

7.1.4 Further analysis of node classification

While the scenarios without measuring noise show a high accuracy, scenarios with noise have a larger dispersion in the matrices that have been discussed in the previous sections. Despite some small changes in fault current that are produced by the different fault resistance values and solar irradiation and temperature conditions, the parameter that has more influence in the test case is the fault type. That means that, for a certain node location, the largest variability among different cases is given by the fault type. Therefore, the results for cases with measuring noise are going to be split in SLG and 3P faults and the results can be appreciated in Figure 12.

Single-Line-to-Ground faults ***3 – Phase faults***

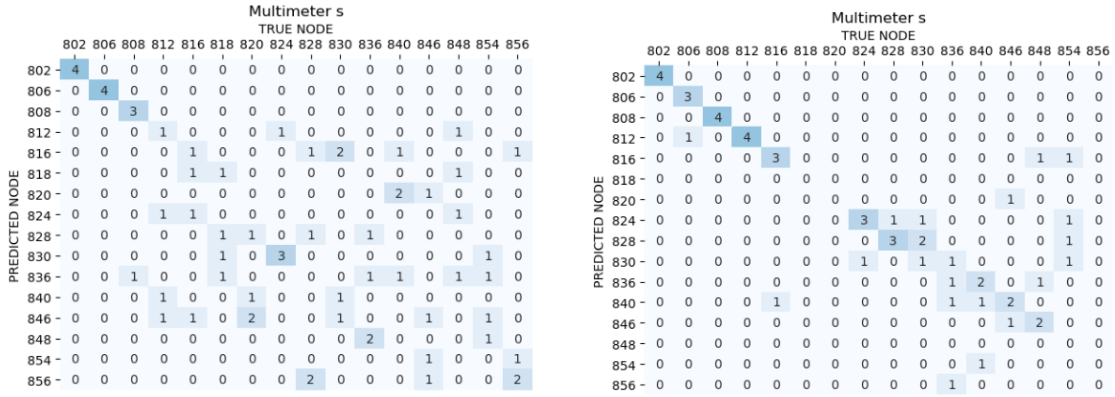

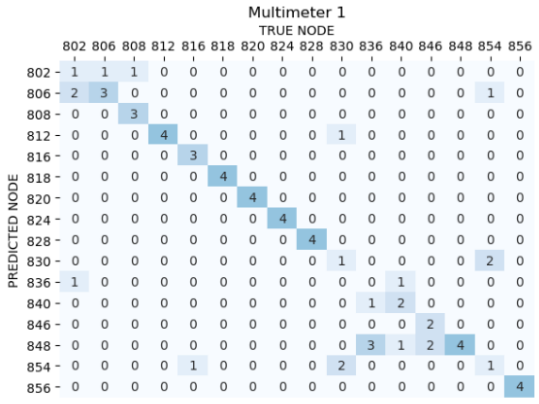
Multimeter 1
TRUE NODE
802 806 808 812 816 818 820 824 828 830 836 840 846 848 854 856
PREDICTED NODE
802 1 1 1 0 0 0 0 0 0 0 0 0 0 0 0 0
806 2 3 0 0 0 0 0 0 0 0 0 0 0 0 1 0
808 0 0 3 0 0 0 0 0 0 0 0 0 0 0 0 0
812 0 0 0 4 0 0 0 0 0 1 0 0 0 0 0 0
816 0 0 0 0 3 0 0 0 0 0 0 0 0 0 0 0
818 0 0 0 0 0 4 0 0 0 0 0 0 0 0 0 0
820 0 0 0 0 0 0 4 0 0 0 0 0 0 0 0 0
824 0 0 0 0 0 0 0 4 0 0 0 0 0 0 0 0
828 0 0 0 0 0 0 0 0 4 0 0 0 0 0 0 0
830 0 0 0 0 0 0 0 0 0 1 0 0 0 0 2 0
836 1 0 0 0 0 0 0 0 0 0 1 0 0 0 0 0
840 0 0 0 0 0 0 0 0 0 0 1 2 0 0 0 0
846 0 0 0 0 0 0 0 0 0 0 0 0 2 0 0 0
848 0 0 0 0 0 0 0 0 0 0 3 1 2 4 0 0
854 0 0 0 0 1 0 0 0 0 2 0 0 0 0 1 0
856 0 0 0 0 0 0 0 0 0 0 0 0 0 0 0 4

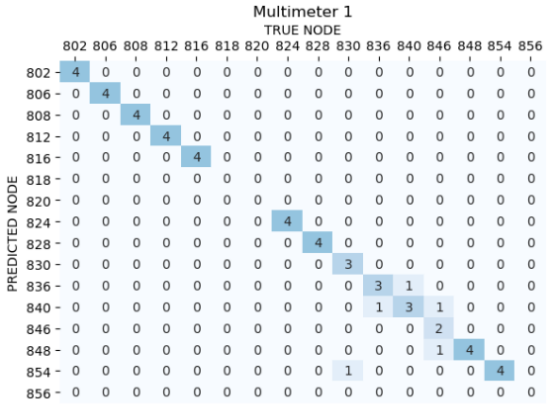
Multimeter 1
TRUE NODE
802 806 808 812 816 818 820 824 828 830 836 840 846 848 854 856
PREDICTED NODE
802 4 0 0 0 0 0 0 0 0 0 0 0 0 0 0 0
806 0 4 0 0 0 0 0 0 0 0 0 0 0 0 0 0
808 0 0 4 0 0 0 0 0 0 0 0 0 0 0 0 0
812 0 0 0 4 0 0 0 0 0 0 0 0 0 0 0 0
816 0 0 0 0 4 0 0 0 0 0 0 0 0 0 0 0
818 0 0 0 0 0 0 0 0 0 0 0 0 0 0 0 0
820 0 0 0 0 0 0 0 0 0 0 0 0 0 0 0 0
824 0 0 0 0 0 0 0 4 0 0 0 0 0 0 0 0
828 0 0 0 0 0 0 0 0 4 0 0 0 0 0 0 0
830 0 0 0 0 0 0 0 0 0 3 0 0 0 0 0 0
836 0 0 0 0 0 0 0 0 0 0 3 1 0 0 0 0
840 0 0 0 0 0 0 0 0 0 0 1 3 1 0 0 0
846 0 0 0 0 0 0 0 0 0 0 0 0 2 0 0 0
848 0 0 0 0 0 0 0 0 0 0 0 0 1 4 0 0
854 0 0 0 0 0 0 0 0 0 0 1 0 0 0 4 0
856 0 0 0 0 0 0 0 0 0 0 0 0 0 0 0 0

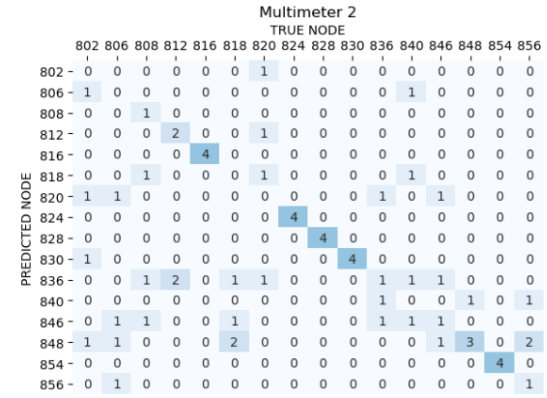
Multimeter 2
TRUE NODE
802 806 808 812 816 818 820 824 828 830 836 840 846 848 854 856
PREDICTED NODE
802 0 0 0 0 0 0 1 0 0 0 0 0 0 0 0 0
806 1 0 0 0 0 0 0 0 0 0 0 1 0 0 0 0
808 0 0 1 0 0 0 0 0 0 0 0 0 0 0 0 0
812 0 0 0 2 0 0 1 0 0 0 0 0 0 0 0 0
816 0 0 0 0 4 0 0 0 0 0 0 0 0 0 0 0
818 0 0 1 0 0 0 1 0 0 0 0 1 0 0 0 0
820 1 1 0 0 0 0 0 0 0 0 1 0 1 0 0 0
824 0 0 0 0 0 0 0 4 0 0 0 0 0 0 0 0
828 0 0 0 0 0 0 0 0 4 0 0 0 0 0 0 0
830 1 0 0 0 0 0 0 0 0 4 0 0 0 0 0 0
836 0 0 1 2 0 1 1 0 0 0 1 1 1 0 0 0
840 0 0 0 0 0 0 0 0 0 0 1 0 0 1 0 1
846 0 1 1 0 0 1 0 0 0 0 1 1 1 0 0 0
848 1 1 0 0 0 2 0 0 0 0 0 0 1 3 0 2
854 0 0 0 0 0 0 0 0 0 0 0 0 0 0 4 0
856 0 1 0 0 0 0 0 0 0 0 0 0 0 0 0 1

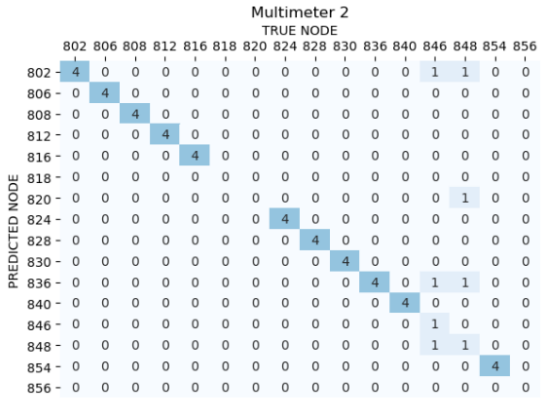
Multimeter 2
TRUE NODE
802 806 808 812 816 818 820 824 828 830 836 840 846 848 854 856
PREDICTED NODE
802 4 0 0 0 0 0 0 0 0 0 0 0 1 1 0 0
806 0 4 0 0 0 0 0 0 0 0 0 0 0 0 0 0
808 0 0 4 0 0 0 0 0 0 0 0 0 0 0 0 0
812 0 0 0 4 0 0 0 0 0 0 0 0 0 0 0 0
816 0 0 0 0 4 0 0 0 0 0 0 0 0 0 0 0
818 0 0 0 0 0 0 0 0 0 0 0 0 0 0 0 0
820 0 0 0 0 0 0 0 0 0 0 0 0 0 1 0 0
824 0 0 0 0 0 0 0 4 0 0 0 0 0 0 0 0
828 0 0 0 0 0 0 0 0 4 0 0 0 0 0 0 0
830 0 0 0 0 0 0 0 0 0 4 0 0 0 0 0 0
836 0 0 0 0 0 0 0 0 0 0 4 0 1 1 0 0
840 0 0 0 0 0 0 0 0 0 0 0 4 0 0 0 0
846 0 0 0 0 0 0 0 0 0 0 0 0 1 0 0 0
848 0 0 0 0 0 0 0 0 0 0 0 0 1 1 0 0
854 0 0 0 0 0 0 0 0 0 0 0 0 0 0 4 0
856 0 0 0 0 0 0 0 0 0 0 0 0 0 0 0 0

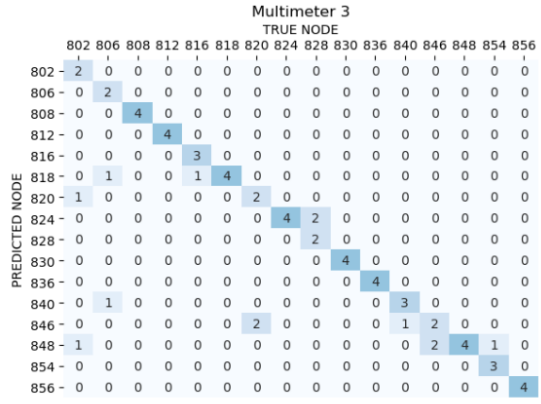
Multimeter 3
TRUE NODE
802 806 808 812 816 818 820 824 828 830 836 840 846 848 854 856
PREDICTED NODE
802 2 0 0 0 0 0 0 0 0 0 0 0 0 0 0 0
806 0 2 0 0 0 0 0 0 0 0 0 0 0 0 0 0
808 0 0 4 0 0 0 0 0 0 0 0 0 0 0 0 0
812 0 0 0 4 0 0 0 0 0 0 0 0 0 0 0 0
816 0 0 0 0 3 0 0 0 0 0 0 0 0 0 0 0
818 0 1 0 0 1 4 0 0 0 0 0 0 0 0 0 0
820 1 0 0 0 0 0 2 0 0 0 0 0 0 0 0 0
824 0 0 0 0 0 0 0 4 2 0 0 0 0 0 0 0
828 0 0 0 0 0 0 0 0 2 0 0 0 0 0 0 0
830 0 0 0 0 0 0 0 0 0 4 0 0 0 0 0 0
836 0 0 0 0 0 0 0 0 0 0 4 0 0 0 0 0
840 0 1 0 0 0 0 0 0 0 0 0 3 0 0 0 0
846 0 0 0 0 0 0 2 0 0 0 0 1 2 0 0 0
848 1 0 0 0 0 0 0 0 0 0 0 0 2 4 1 0
854 0 0 0 0 0 0 0 0 0 0 0 0 0 0 3 0
856 0 0 0 0 0 0 0 0 0 0 0 0 0 0 0 4

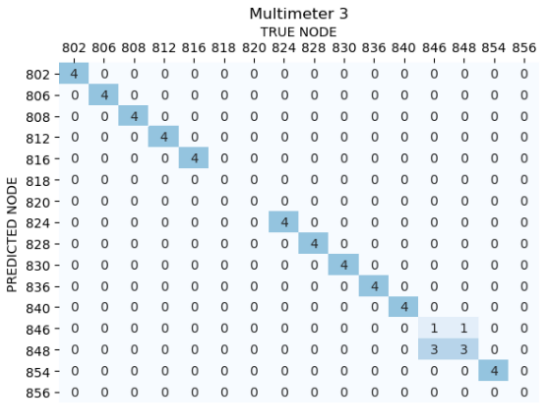
Multimeter 3
TRUE NODE
802 806 808 812 816 818 820 824 828 830 836 840 846 848 854 856
PREDICTED NODE
802 4 0 0 0 0 0 0 0 0 0 0 0 0 0 0 0
806 0 4 0 0 0 0 0 0 0 0 0 0 0 0 0 0
808 0 0 4 0 0 0 0 0 0 0 0 0 0 0 0 0
812 0 0 0 4 0 0 0 0 0 0 0 0 0 0 0 0
816 0 0 0 0 4 0 0 0 0 0 0 0 0 0 0 0
818 0 0 0 0 0 0 0 0 0 0 0 0 0 0 0 0
820 0 0 0 0 0 0 0 0 0 0 0 0 0 0 0 0
824 0 0 0 0 0 0 0 4 0 0 0 0 0 0 0 0
828 0 0 0 0 0 0 0 0 4 0 0 0 0 0 0 0
830 0 0 0 0 0 0 0 0 0 4 0 0 0 0 0 0
836 0 0 0 0 0 0 0 0 0 0 4 0 0 0 0 0
840 0 0 0 0 0 0 0 0 0 0 0 4 0 0 0 0
846 0 0 0 0 0 0 0 0 0 0 0 0 1 1 0 0
848 0 0 0 0 0 0 0 0 0 0 0 0 3 3 0 0
854 0 0 0 0 0 0 0 0 0 0 0 0 0 0 4 0
856 0 0 0 0 0 0 0 0 0 0 0 0 0 0 0 0

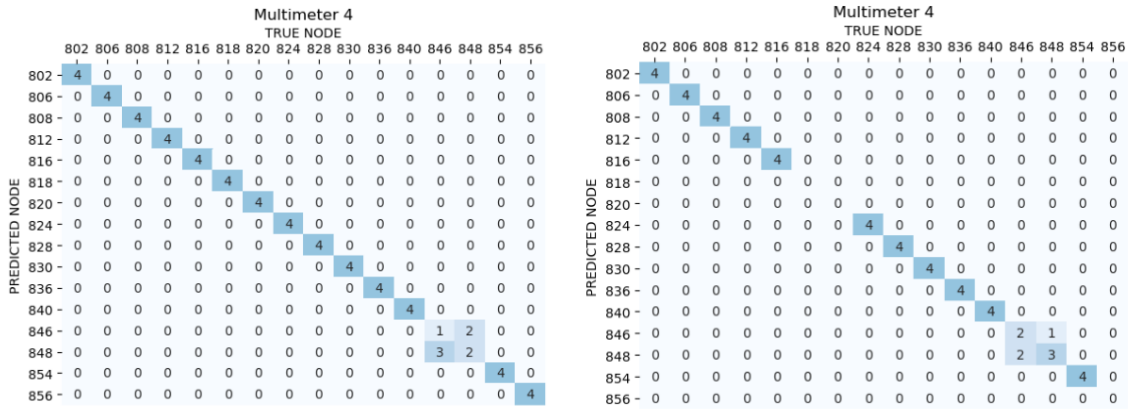

Figure 12. Node classification results for cases with noise split by type

From the results that are presented in the matrices above, it is possible to conclude that matrices for SLG faults only show more dispersion. That means that SLG faults are more prone to be classified in the wrong node.

7.2 Type classification

In this case, the confusion only has two labels, which are the two studied fault types (Single-Line-to-Ground faults, ‘SLG’, and three-phase faults, ‘3P’).

7.2.1 Without noise

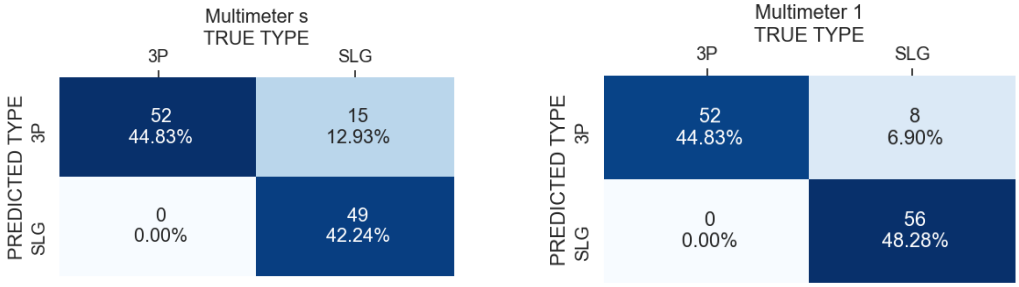

Accuracy: 87.07%

Accuracy: 93.11%

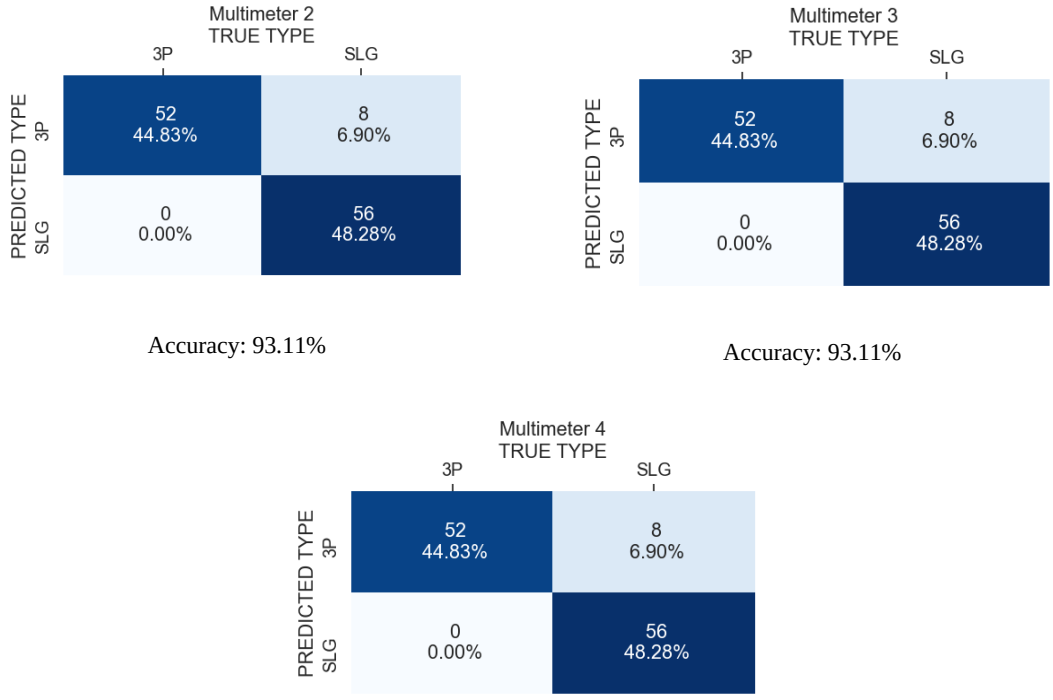

Figure 13. Type classification results for cases without noise

In Figure 13, it is possible to appreciate that type classification in without noise scenarios shows a really high accuracy (93.11%) for the multimeters located across the system. For the multimeter located on the substation, accuracy is a little bit lower (87.07%). It is remarkable that 4 out of 5 multimeters are able to classify correctly the same number of faults. This can be easily explained by looking at the patterns of the traveling waves, which are quite different for SLG and 3P faults. Therefore, frequency components will different enough as well and classifying any new fault by type becomes an easy task.

For the multimeter in the substation, most of the misclassifications are concentrated on nodes 846 and 848, although there are other occasional errors on nodes 808, 828 and 840. For other multimeters, errors mainly come from nodes 846 and 848. A summary of those nodes where misclassification takes place can be observed in Figure 14.

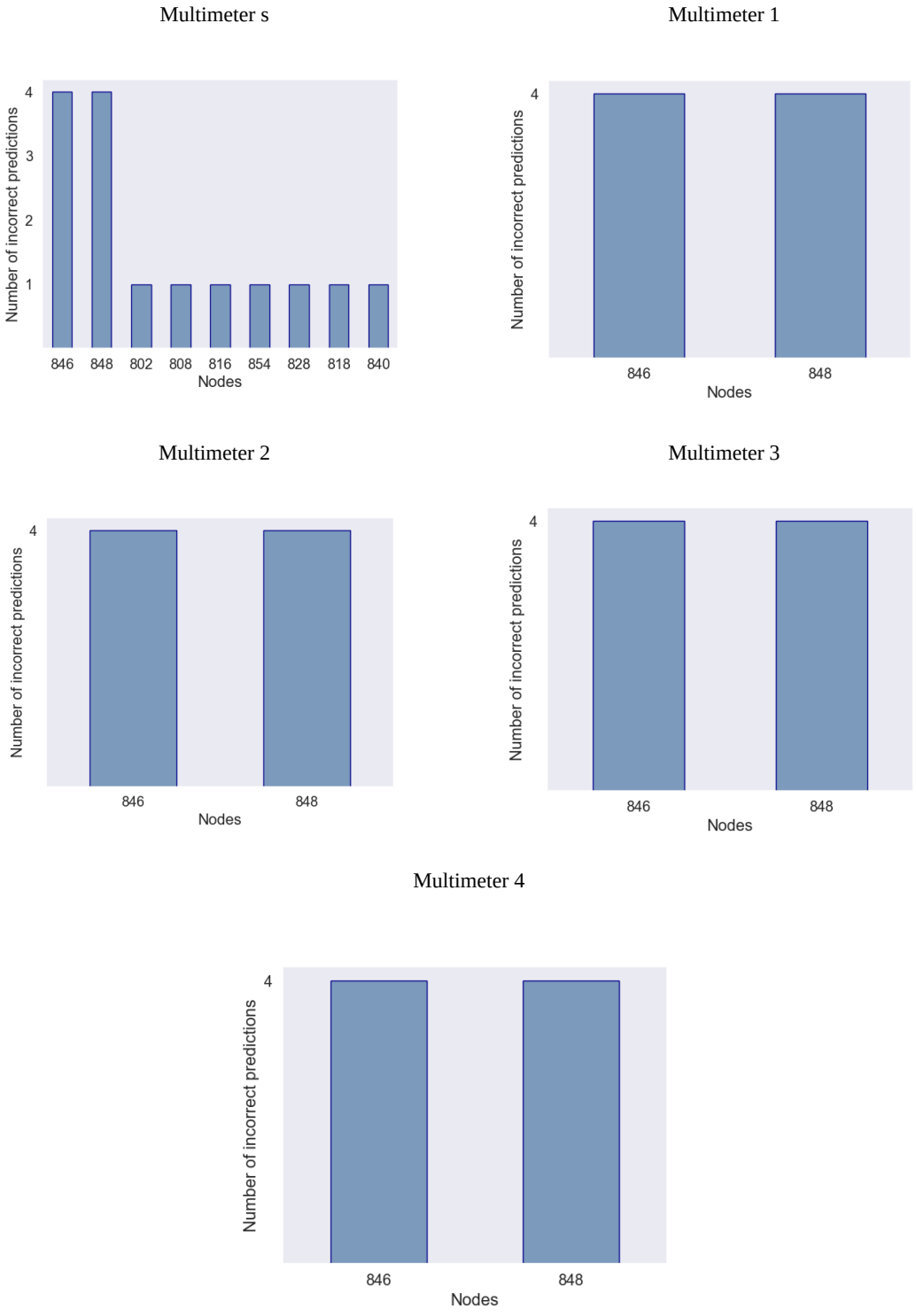

Figure 14. Nodes where incorrect predictions in type classification take place in cases without noise

7.2.2 With noise

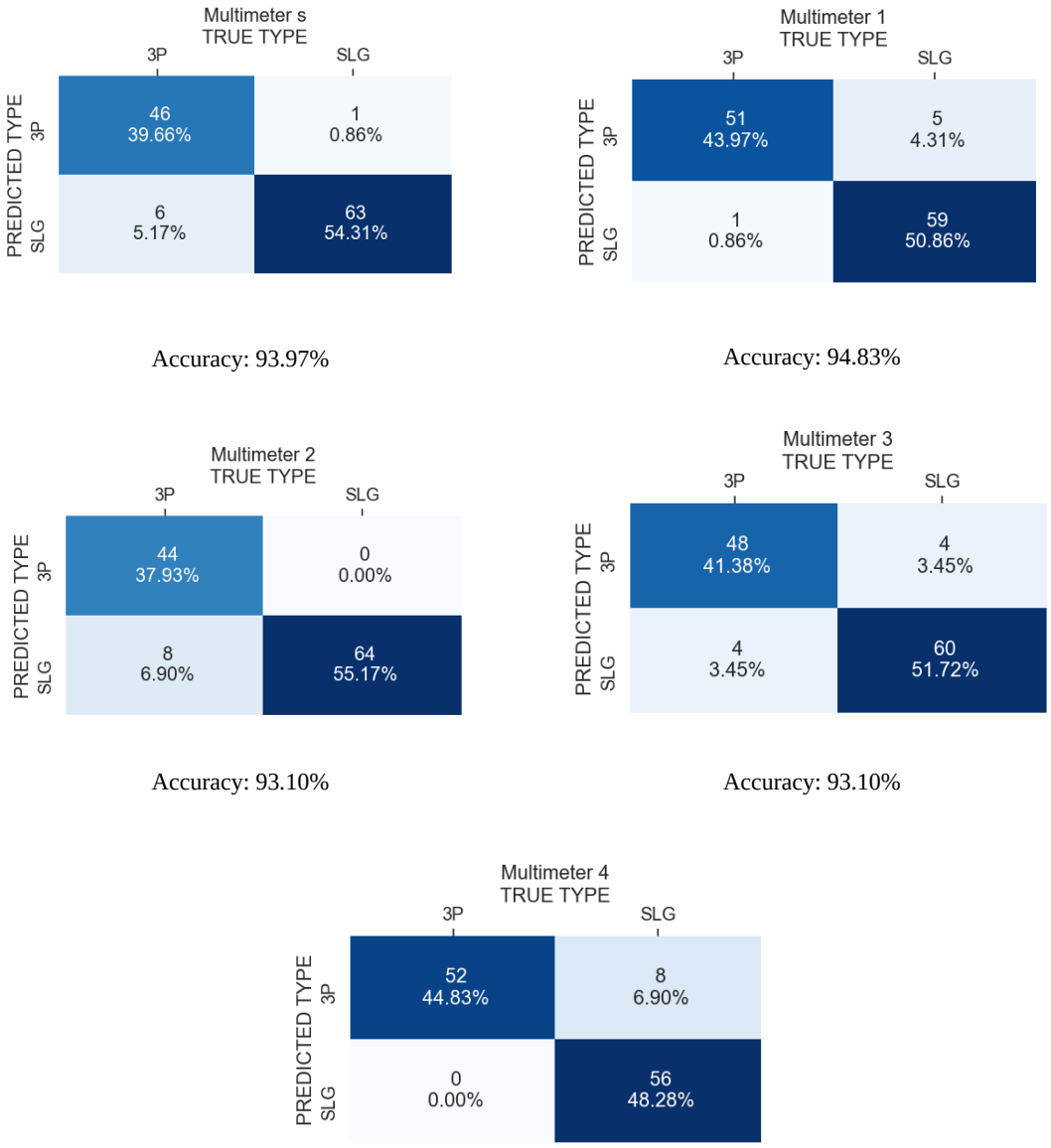

Figure 15. Type classification results for cases with noise

Paradoxically, as it can be observed in Figure 15, cases with noise obtain higher accuracy than cases without noise in multimeter 1 and in the multimeter located in the

substation. This result could be motivated by the level of noise that is added to the signal, that in this particular case is beneficial for the CNN model training and evaluation. There still misclassifications on nodes 846 and 848, and even in other nodes such as 840 and 854, but the overall error rate is less for those two multimeters. The summary of nodes where incorrect predictions takes place is included in Figure 16.

For the multimeters 2, 3 and 4, accuracy remains the same as in the cases without noise. These results show the reliability of the method, which is able of maintaining the same accuracy even when the input signals are distorted with high-frequency noise.

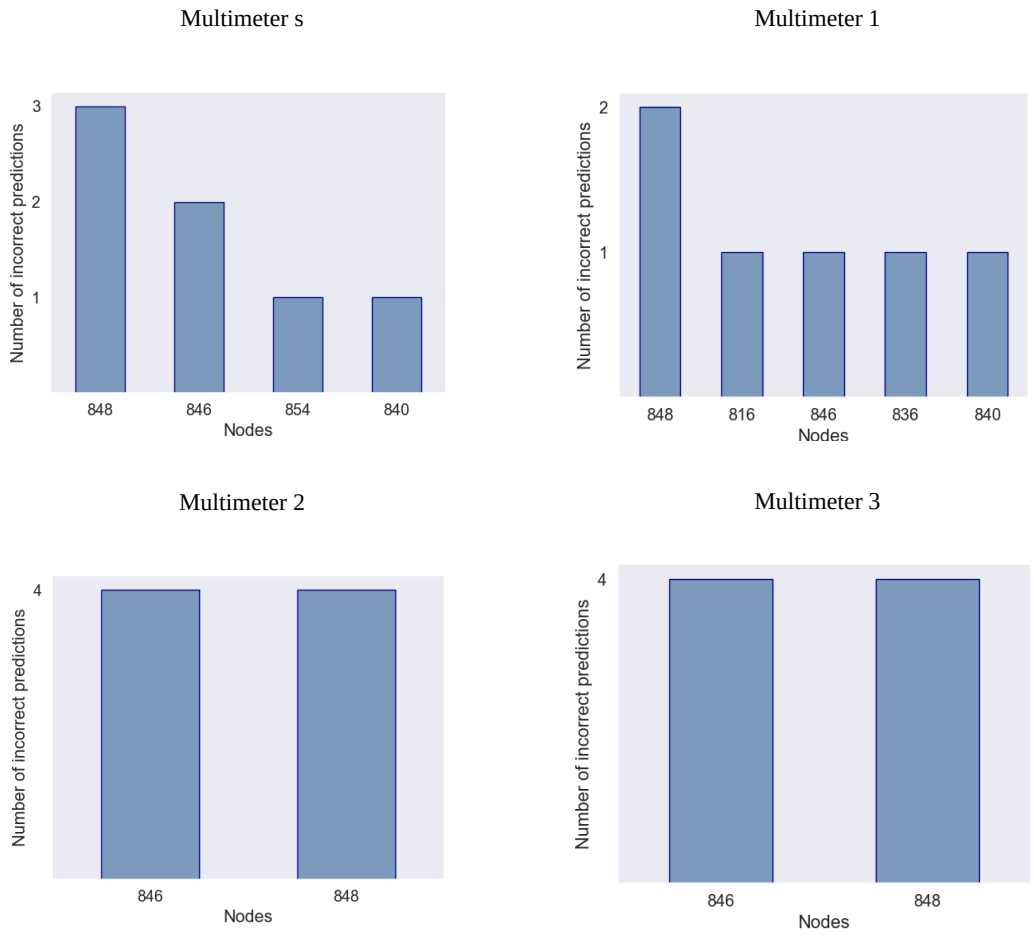

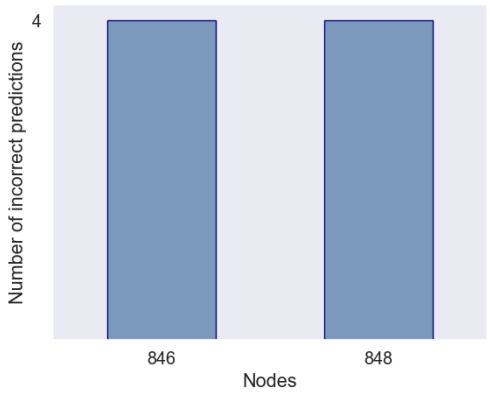

Figure 16. Nodes where incorrect predictions in type classification take place in cases with noise

7.2.3 Further analysis of type classification

In Figure 17, the locations where the type misclassifications take place are shown in the map. It is possible to observe that most of the locations are either distant nodes, specially from the multimeters that misclassified the fault (usually the multimeter in the substation or multimeter 1) or the already know problematic nodes 846 or 846. These last two nodes accumulate most of the cases.

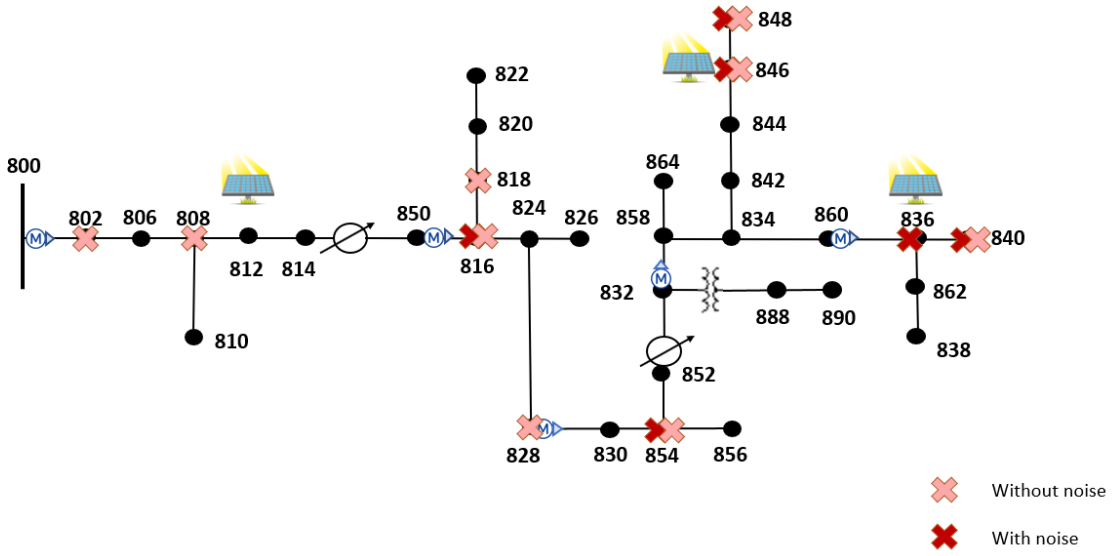

Figure 17. Test system with the locations where incorrect predictions in type classification take place in cases with and without noise

7.3 Further analysis of the model evaluation

Throughout the results that have been previously explained, there is one common topic across all the sections: both type and node misclassification often occur on nodes 846 and 848. Just for information, Figure 18 shows a few plots of traveling waves produced by faults on nodes 846 and 848 from different fault scenarios. Both SLG and 3P faults are included for comparison. The perspectives from different multimeters reinforce the idea that fault signals seem too similar in inherent frequency components and that may be the reason of the multiple misclassifications.

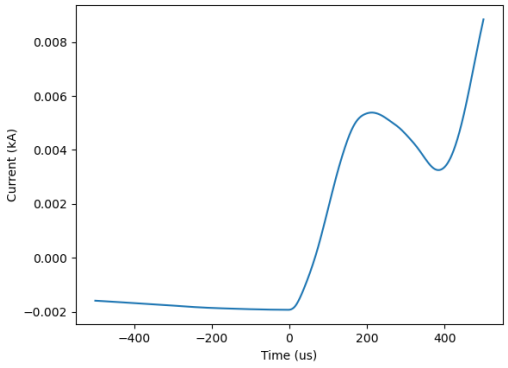

SLG fault on node 846, resistance 10 Ω, irradiation 1000 W/m^2, temperature 50°C. Measured in Multimeter 2.

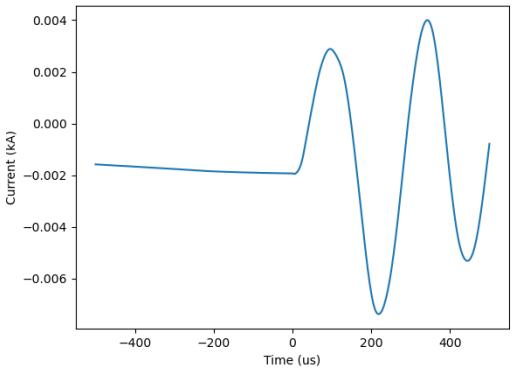

3P fault on node 846, resistance 10 Ω, irradiation 1000 W/m^2, temperature 50°C. Measured in Multimeter 2.

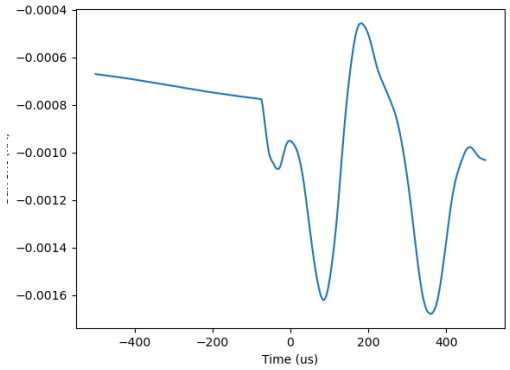

SLG fault on node 846, resistance 0.01 Ω, irradiation 600 W/m^2, temperature 28°C. Measured in Multimeter 4.

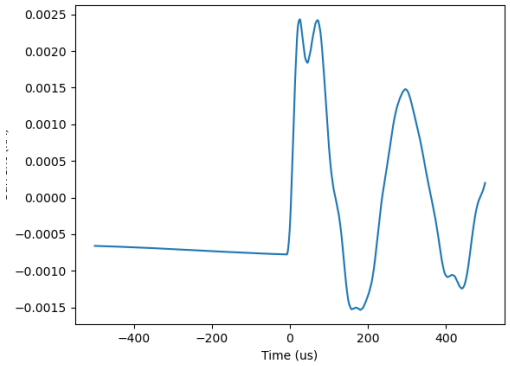

3P fault on node 846, resistance 0.01 Ω, irradiation 600 W/m^2, temperature 28°C. Measured in Multimeter 4.

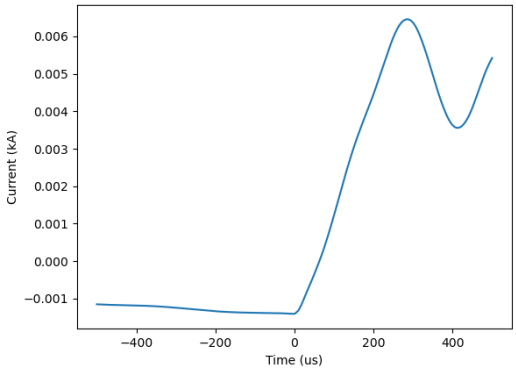

SLG fault on node 848, resistance 10 Ω, irradiation 600 W/m^2, temperature 50°C. Measured in Multimeter 3.

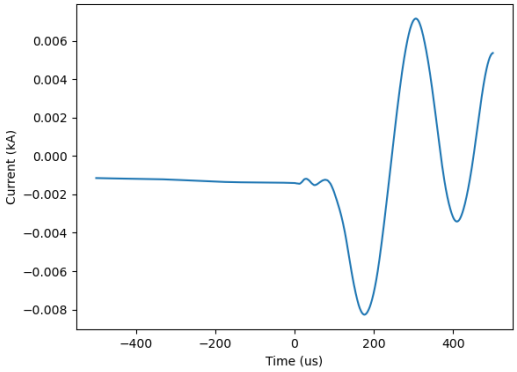

3P fault on node 848, resistance 10 Ω, irradiation 600 W/m^2, temperature 50°C. Measured in Multimeter 3.

Figure 18. Faults on node 846 and 848

Next figure shows a few traveling waves originated by faults in other nodes. As it can be appreciated, the signals seem to contain high frequency components, that signals from nodes 846 and 848 seem to be lacking.

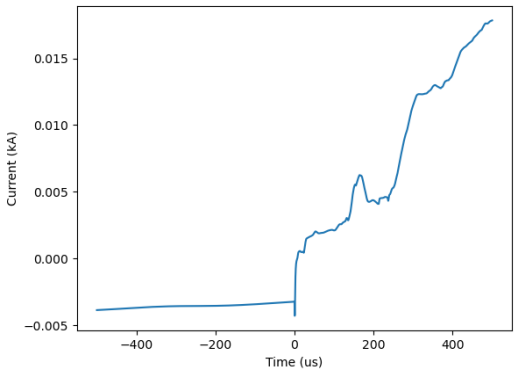

SLG fault on node 828, resistance 1 Ω, irradiation 1000 W/m^2, temperature 50°C. Measured in Multimeter 1.

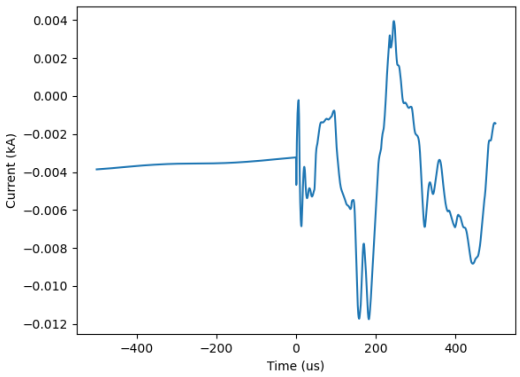

3P fault on node 828, resistance 1 Ω, irradiation 1000 W/m^2, temperature 50°C. Measured in Multimeter 1.

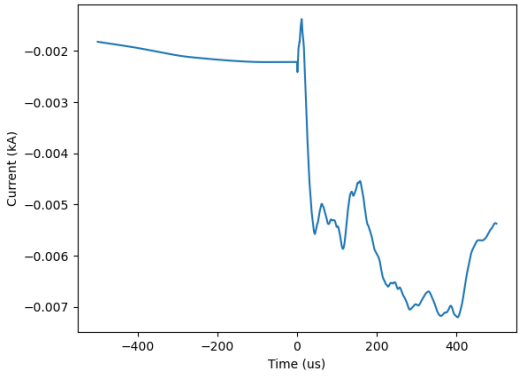

SLG fault on node 802, resistance 10 Ω, irradiation 1000 W/m^2, temperature 28°C. Measured in Multimeter 2.

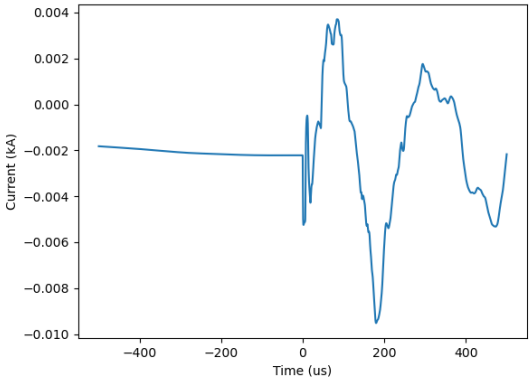

3P fault on node 802, resistance 10 Ω, irradiation 1000 W/m^2, temperature 28°C. Measured in Multimeter 2.

Figure 19. Faults on node 828 and 802

Everything seems to indicate that the capacitor which is located in node 844 is the cause of the smoothness of the signals coming from nodes 846 and 848. The only explanation is that the capacitor is filtering the waves, which provoke the lose of valuable information. This lack of information confuses the algorithm, that is unable to classify correctly most of the faults that took place at the other side of the capacitor.

CHAPTER 8. FUTURE WORK

This project is a first attempt towards a proposed fault classification method, which has been conducted under specific circumstances. The results obtained are promising. However, there are still many research directions that are open to future work.

First, in this project cases with noise and without noise have been studied. For the cases with noise, a single level of noise and a single smoothing window in the preprocessing stage have been used. It would be a great idea to analyze the accuracy sensitivity for different levels of noise (which is more aligned with what happens in reality) and for smoothing windows of different types and lengths.

Second, the method uses frequency vs. time representation of the signals, which is obtained by the CWT, to train the CNNs and classify the faults. According to the propagation theory of traveling waves explained in [5], each fault should display a characteristic frequency spectrum which is shaped by the wave attenuation along the path. Therefore, it should be able to study the frequency components, determine the dominants ones and use them as another classification rule.

Third, one of the advantages of this method is that it uses a minimal amount of information for classifying the fault. It is just 1 ms of current measurements, which is much less than other current protection devices. However, this time window could be optimized so the amount of required information is even smaller, and the algorithm is faster in consequence.

Fourth, the cases on nodes 846 and 848 remain without a clear explanation. It would be a good idea to locate a multimer in the other side of the node 844 and try to perform

again the classification of the faults. In that way, the relevant frequency components are not filtered out and a satisfactory performance should be achievable.

Another important expansion point is to consider faults between nodes (i.e., in the middle of the lines). This method doesn't aim (and doesn't have the capability) to calculate the exact location of the fault within a line, however, it would be very interesting in terms of a practical application to point out that a fault has occurred in a line. Later, other methods could be deployed to calculate the exact location where the fault took place.

Furthermore, in terms of pursuing a real application, this method should be able to discern when sudden changes in currents are related to faults and when not. For example, the change of a tap in a regulator or the opening/closing of a regulator bank could introduce high-frequency noise in the ground mode current that could be considered as a fault. These events should be incorporated to the study and another preprocessing stage or another class in the classification algorithm should be devoted to identifying them.

Lastly, both type and node CNNs follow the same layer structure. An optimization of the used layers, such as the number of layers, the number of neurons, the layer types, … could be performed to achieve further gains in accuracy.

CHAPTER 9. CONCLUSIONS

This thesis addresses the task of fault classification (node location and fault type) for a distribution system with high penetration of PV. The simulated fault events include different combinations of irradiance and temperature for the PV systems and different fault resistances. In order to study the suitability of the method for a real application, the same events with an added gaussian noise have been considered as well.

The first stage of the proposed method is the detection of the fault event. In order to perform a fast detection, the algorithm infers the presence of a fault by the detection of the produced traveling wave. The CWT is employed to analyze the signal. Any change in the signal frequency components will be reflected on the CWT coefficient matrices. Analyzing these coefficients for the highest frequencies it is possible to determine if a fault has occurred. In the cases with noise, a smoothing filter is employed to remove the high frequency components which related to the noise from the signal.

The second step is to use the CWT coefficient matrices of the traveling waves to train two Convolutional Neural Networks to predict both the fault node and the type of the fault in a per-multimeter basis. The results suggest that the CNN is a promising tool able to extract features from the matrices, which leads to a great performance in fault classification. In the scenarios without noise, results show that node prediction accuracy is over 80%, being around 95% for four out of five multimeters. For fault type prediction, it is around 90% for all the multimeters.

For cases with noise, node classification accuracies are lower in general. Specially, the accuracy in the multimeter located at the substation is severely impacted, which suggest that classification based on wave frequency components is less effective for distant faults in noisy scenarios. However, for all the multimeters, it is possible to define an area around

them in which accuracy levels are high. Also, it is remarkable that most of the misclassifications are related to SLG faults rather than to 3P faults. Nodes included in those areas conform the so-called “protection zones.” On the contrary, accuracy levels for type classification remains the same or even increase for some of the multimeters.

For both noise and without noise scenarios, misclassifications are prone to occur for faults in the nodes 846 and 848. The recorded waveforms are very different from other faults simulated in other nodes. The most probable explanation is the filtering effect that the capacitor on node 844 could have on the waves, that produce a loss of frequency components and therefore, relevant information.

Although this method needs more research before it is deployed on a real application, the satisfactory results that are obtained in this project are enough to validate the defined goals, which were to create a fast fault detection and classification method, applying Machine Learning algorithms, aimed for distribution power systems with high penetration of solar PV.

APPENDIX A. SOLAR FARM MODEL

This is an overall scheme of the solar farm model can be appreciated in the following picture. From right to left, the first grey element are the irradiation and temperature controls. Before taking each snapshot and before doing the simulation, these blocks have to adjusted. Irradiation and temperature go directly into the PV array block.

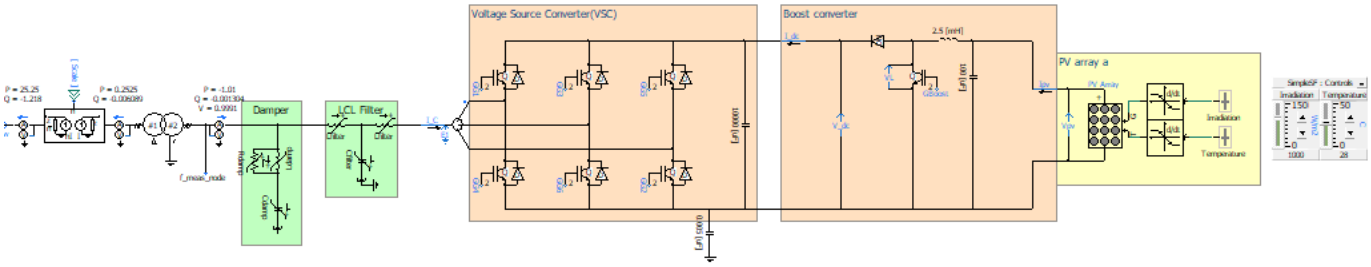

Figure 20. Overall representation of the solar farm model

The PV array block (yellow) allows to tune the size of the PV array: number of cells, strings... The employed values are included in Figure 21.

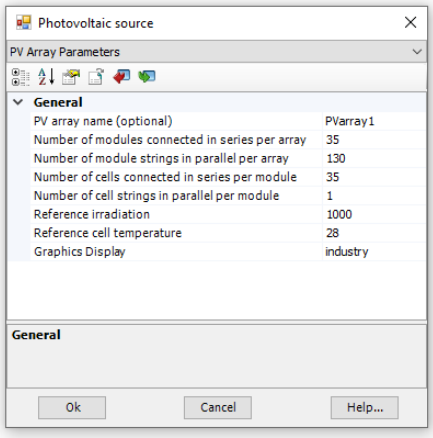

Figure 21. Detail of the parameters in the PV array block

Next, the first orange block is the Boost Converter. The boost converter is a DC/DC converter used to raise the source voltage. The duty factor is given by the MPPT controller in order to achieve the targeted output voltage. As the input and output power has to be the same, output current is regulated as well. The second orange block starting from the right is the inverter, which turns the input DC current into AC, which can be fed into the system.

The following two green blocks are a filter and a damper that are used to remove harmonics before introducing the inverted waveforms into the system. In this way, the output signal will look more sinusoidal and will introduce less distortion.

The final element in the model, situated on the left side, is the scaling component. The solar farm is composed by a certain number of panels. This scaling component multiplies the output by the number of panels to simulate the solar farm. In this case, the solar farm is composed by 2 panels.

REFERENCES

[1] S. S. Gururajapathy, H. Mokhlis and H. A. Illias. “Fault location and detection techniques in power distribution systems with distributed generation: A review,” in Renewable and Sustainable Energy Reviews, Elsevier, vol. 74(C), pages 949-958, 2017.

[2] X. Chen, X. Yin, S. Deng. “A Novel Method for SLG Fault Location in Power Distribution System Using Time Lag of Travelling Wave Components”, in Transactions of Electrical and Electronic Engineering, Institute of Electrical Engineers of Japan, vol. 12, issue 1, pp. 45-54, 2017.

[3] Eyada A. Alanzi, Mahmoud A. Younis, Azrul Mohd Ariffin, “Detection of faulted phase type in distribution systems based on one end voltage measurement”, in International Journal of Electrical Power & Energy Systems, vol. 54, pp. 288-292, 2014.

[4] F. V. Lopes, K. M. Dantas, K. M. Silva and F. B. Costa, "Accurate Two-Terminal Transmission Line Fault Location Using Traveling Waves," in IEEE Transactions on Power Delivery, vol. 33, no. 2, pp. 873-880, April 2018.

[5] A. Borghetti, M. Bosetti, M. Di Silvestro, C. A. Nucci and M. Paolone, "Continuous-Wavelet Transform for Fault Location in Distribution Power Networks: Definition of Mother Wavelets Inferred From Fault Originated Transients," in IEEE Transactions on Power Systems, vol. 23, no. 2, pp. 380-388, May 2008.

[6] A. Borghetti, M. Bosetti, C. A. Nucci, M. Paolone and A. Abur, "Integrated Use of Time-Frequency Wavelet Decompositions for Fault Location in Distribution Networks: Theory and Experimental Validation," in IEEE Transactions on Power Delivery, vol. 25, no. 4, pp. 3139-3146, Oct. 2010.

[7] M. Jamil, R. Singh & S. Sharma. “Fault Identification In Electrical Power Distribution System Using Combined Discrete Wavelet Transform and Fuzzy Logic,” in Journal of Electrical Systems and Information Technology, vol.2, 2015.

[8] Z. Jiao. A New Method to Improve Fault Location Accuracy in Transmission Line Based on Fuzzy Multi-Sensor Data Fusion.

[9] H. Livani and C. Y. Evrenosoğlu, "A Fault Classification and Localization Method for Three-Terminal Circuits Using Machine Learning," in IEEE Transactions on Power Delivery, vol. 28, no. 4, pp. 2282-2290, Oct. 2013.

[10] S. Hongchun, W. Xu, X. Qi, W. Qinjin, T. Xincui. A Fault Location Method of Traveling Wave for Distribution Network with only Two-Phase Current Transformer Using Artificial Neutral Network.

[11] J. Gracia, A. J. Mazon and I. Zamora, "Best ANN structures for fault location in single-and double-circuit transmission lines," in IEEE Transactions on Power Delivery, vol. 20, no. 4, pp. 2389-2395, Oct. 2005.

[12] M. Guo, X. Zeng, D. Chen and N. Yang, "Deep-Learning-Based Earth Fault Detection Using Continuous Wavelet Transform and Convolutional Neural Network in Resonant Grounding Distribution Systems," in IEEE Sensors Journal, vol. 18, no. 3, pp. 1291-1300, Feb. 2018.

[13] S. Lan, M. Chen and D. Chen. “A Novel HVDC Double-Terminal Non-Synchronous Fault Location Method Based on Convolutional Neural Network,” in IEEE Transactions on Power Delivery, 2019.

[14] J. Liang, T. Jing, H. Niu and J. Wang, "Two-Terminal Fault Location Method of Distribution Network Based on Adaptive Convolution Neural Network," in IEEE Access, vol. 8, pp. 54035-54043, 2020

[15] A. Tabatabaei, M. R. Mosavi and P. Farajiparvar. A Traveling-Wave Fault Location Technique for Three-Terminal Lines Based on Wavelet Analysis and Recurrent Neural Network Using GPS Timing.

[16] M. N. Hashim, M. K. Osman, M. N. Ibrahim, A. F. Abidin and M. N. Mahmud, "Single-ended fault location for transmission lines using traveling wave and multilayer perceptron network," 2016 6th IEEE International Conference on Control System, Computing and Engineering (ICCSCE), Batu Ferringhi, 2016, pp. 522-527.

[17] Y. Q. Chen, O. Fink and G. Sansavini. “Combined Fault Location and Classification for Power Transmission Lines Fault Diagnosis With Integrated Feature Extraction,” in IEEE Transactions on Industrial Electronics, vol. 65, pp. 561-561, 2018.

[18] PSCAD Q&A, IEEE 34 bus example. Available at: https://forum.hvdc.ca/833005/IEEE-34-bus-example

[19] Distribution System Analysis Subcommittee. Radial Distribution Test Feeders.

[20] Distribution System Analysis Subcommittee. IEEE 34 Node Test Feeder.

[21] PSCAD Knowledge Base, Simple Solar Farm. Available at: https://www.pscad.com/knowledge-base/article/521

[22] E. Muljadi, M. Singh, and V. Gevorgian. "PSCAD Modules Representing PV Generator." National Renewable Energy Laboratory (NREL), August 2013.

[23] H. Jia. "An Improved Traveling-Wave-Based Fault Location Method with Compensating the Dispersion Effect of Traveling Wave in Wavelet Domain," in Mathematical Problems in Engineering, 2017.